DETRITAL THERMOCHRONOLOGY ($^{40}AR/^{39}AR$) OF THE RANGIT WINDOW, SIKKIM HIMALAYA

Michael Doon

Submitted in Partial Fulfillment of the Requirements

for the Degree of Bachelor of Science, Honours

Department of Earth Sciences

Dalhousie University, Halifax, Nova Scotia

March 2010

DALHOUSIE UNIVERSITY
Inspiring Minds

Department of Earth Sciences
Halifax, Nova Scotia
Canada B3H 4J1
(902) 494-2358
FAX (902) 494-6889

DATE: May 26, 2010

AUTHOR: Michael Doon

TITLE: Detrital Thermochronology ($^{40}Ar/^{39}Ar$) of the Rangit Window, Sikkim Himalaya

Degree: B. Sc Honours Convocation: May Year: 2010

Permission is herewith granted to Dalhousie University to circulate and to have copied for non-commercial purposes, at its discretion, the above title upon the request of individuals or institutions.

Signature of Author

Acknowledgements

I would like to acknowledge and thank Djordje Grujic for his patience and time, as he was an asset in completing this thesis, and was always made time available for discussion. I would also like to thank Keith Taylor of the Argon Isotope lab for his contribution to this thesis. Without Keith there would be no data. Other people I would like to thank are: Matt Cliffer, Charlie Walls, Peter Reynolds, and Nick Whynot. Finally I would like to thank my roommates for their patience the last few weeks of this thesis, and my parents, for all of their love and support.

Abstract

The Gondwana Formation (GF) is a poorly understood lithological unit at the base of the Lesser Himalayan Sequence (LHS), with a poorly constrained Permian age. West of Nepal and East of Bhutan, in the Sikkim region of India, tectonics and perhaps river incision influenced the formation of a double tectonic window revealing micaceous sandstones of the GF in the core. Bounded by the Main Central Thrust (MCT) at the base, and the Ramgarh Thrust in the roof, the area has undergone a great amount of deformation resulting in a transverse antiform of the LHS. Such structures are rare in the Himalayas and one hypothesis states that these structures are the result of interaction between tectonics (Himalayan collision) and focused erosion (incision of the largest Himalayan rivers). Using ^{40}Ar / ^{39}Ar dating of detrital muscovite grains from GF, the provenance of GF and its thermal and structural history will be interpreted. Combined with a concomitant study using other themochronometers this study will determine exhumation rates in the window and thus help determine the relative importance of focused river incision and localized tectonic deformation. Preliminary ages suggest that the temperatures caused by Tertiary Himalayan metamorphism and tectonic burial were not high enough to reset the ^{40}Ar / ^{39}Ar ages of the muscovite grains. This puts a constraint on maximal temperatures and therefore burial attained by the GF.

TABLE OF CONTENTS

Page

TABLE OF FIGURES

TABLE OF TABLES

CHAPTER 1 INTRODUCTION

The collision of Eurasian and Indian plates began ~50.5 Ma (Zhu et al., 2005), which started the orogenesis of the Himalayan Mountain range and growth of the Tibetan plateau. The ongoing convergence caused a huge amount of crustal material to become deformed and buried, subjecting it to increasing temperature and pressure. Millions of years of tectonic and erosional processes have resulted in the first-order features of the Himalayas such as the crustal scale shear zones running along entire length of the orogen. Smaller structures, such as transverse anticlines appear less important. The Himalayas show a general E-W trend to both structures and lithotectonic units. There are also several anticlines that have approximate N-S trends, which have resulted in tectonic windows and half windows. These structures are an "anomaly" as the process of how they are formed is still being debated but may provide important information how the Himalayas evolved. The trend of these structures is parallel to the shortening direction in the Himalayas, so the question is how, when and why were these transverse anticlines, suggesting E-W direction of shortening, formed. One end member possibility is through purely tectonic processes, or the second possibility through focused erosion along major Himalayan rivers and localized rock uplift.

The mechanism of erosion that will be investigated is focused river incision in the Sikkim Himalaya, and its effect on the local rate of exhumation of the lithological units. The tectonic structure that will be examined is a double tectonic window, a large half window with a closed window located within, which exposes the core of a transverse antiform, along which a large river and one of its tributaries flow.

In this thesis I will apply the $^{40}Ar/^{39}Ar$ dating method on detrital muscovite grains from the late Paleozoic Gondwana Formation (GF) of the Lesser Himalayan Sequence that has been exposed in the double window. The Gondwana formation is the structurally lowest unit of the Himalaya, therefore this dating method will determine: (a) if the tectonic burial of the GF increased the temperatures over the closure temperature of the ^{40}Ar / ^{39}Ar system, and when the rocks cooled below it during the succeeding exhumation, or (b) the initial age of the detrital muscovite and thus provide information about the provenance of the sediment of the GF.

Using other low temperature thermochronometers (e.g. apatite fission-track dating) from a related study by Dr. I. Coutand, the exhumation rates of the tectonic double window is determined and which helps determine the importance of focused river incision and localized tectonic deformation (i.e. folding or localized duplexing, e.g. McQuarrie et al., 2008). This information can be used to understand whether or not river incision acts as an accelerant for localized rock uplift and could possibly create structures such as transverse antiforms as suggested by Montgomery and Stolar (2006).

CHAPTER 2 BACKGROUND

2.1. Regional Geology

Within the Sikkim Himalaya from south to north, the main stratigraphic units and faults are the Main Frontal thrust (MFT), Sub-Himalayan strata, Main Boundary Thrust (MBT), Lesser Himalayan Sequence (LHS), Ramgarh Thrust (RT), Main Central Thrust (MCT), Greater Himalayan Sequence (GHS), South Tibetan Detachment system (STD) and the Tethyan sedimentary sequence (Bhattacharya and Mitra, 2009) (Figure 2.1). The RT and MCT are the structures that define the Tista window (TW) and Rangit window (RW), which are the components of the double tectonic window that will be discussed further in this chapter.

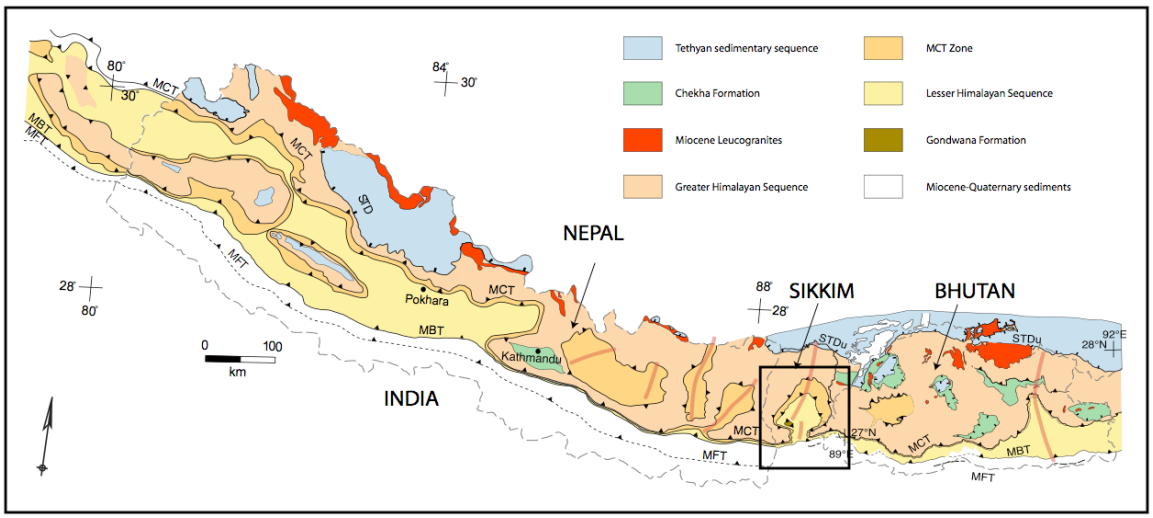

Figure 2.1. Geologic map of India, Nepal and Bhutan portions of the Himalayan orogen with red lines indicating several axial traces of transverse antiforms, modified after McQuarrie et al. 2008. MFT - Main frontal Thrust; MBT – Main Boundary Thrust; MCT- Main Central Thrust; STD - South Tibetan Detachment. Study area outlined in black (Figure 2.2).

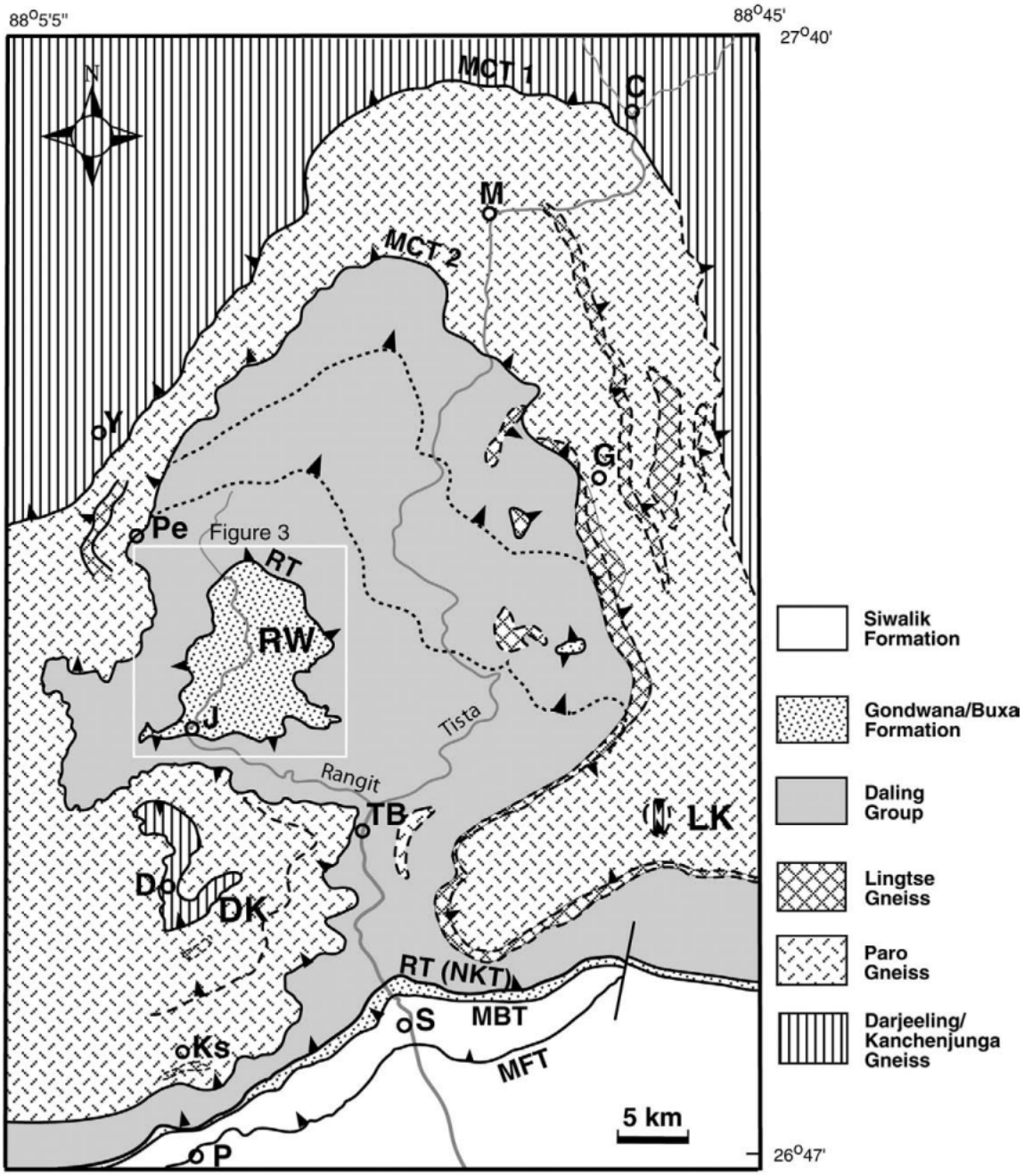

Figure 2.2 Regional map of the Darjeeling – Sikkim Himalaya (DSH), after Bhattacharyya and Mitra, 2009. In the DSH, both the MCT 1 and MCT 2 sheets are translated southward to within 5 km of the Himalayan mountain front and are exposed in the Darjeeling (DK) and the Labha klippen (LK). The Rangit window (RW) lies north of the Darjeeling klippe. The main faults are labeled (see text for details). Towns shown are: C — Chungthang; D — Darjeeling; G — Gangtok; J — Jor khabari; Pe — Pelling ; S — Sevok; TB — Teesta Bazaar; and Y — Yuksom. Figure 2.3 outlined in white.

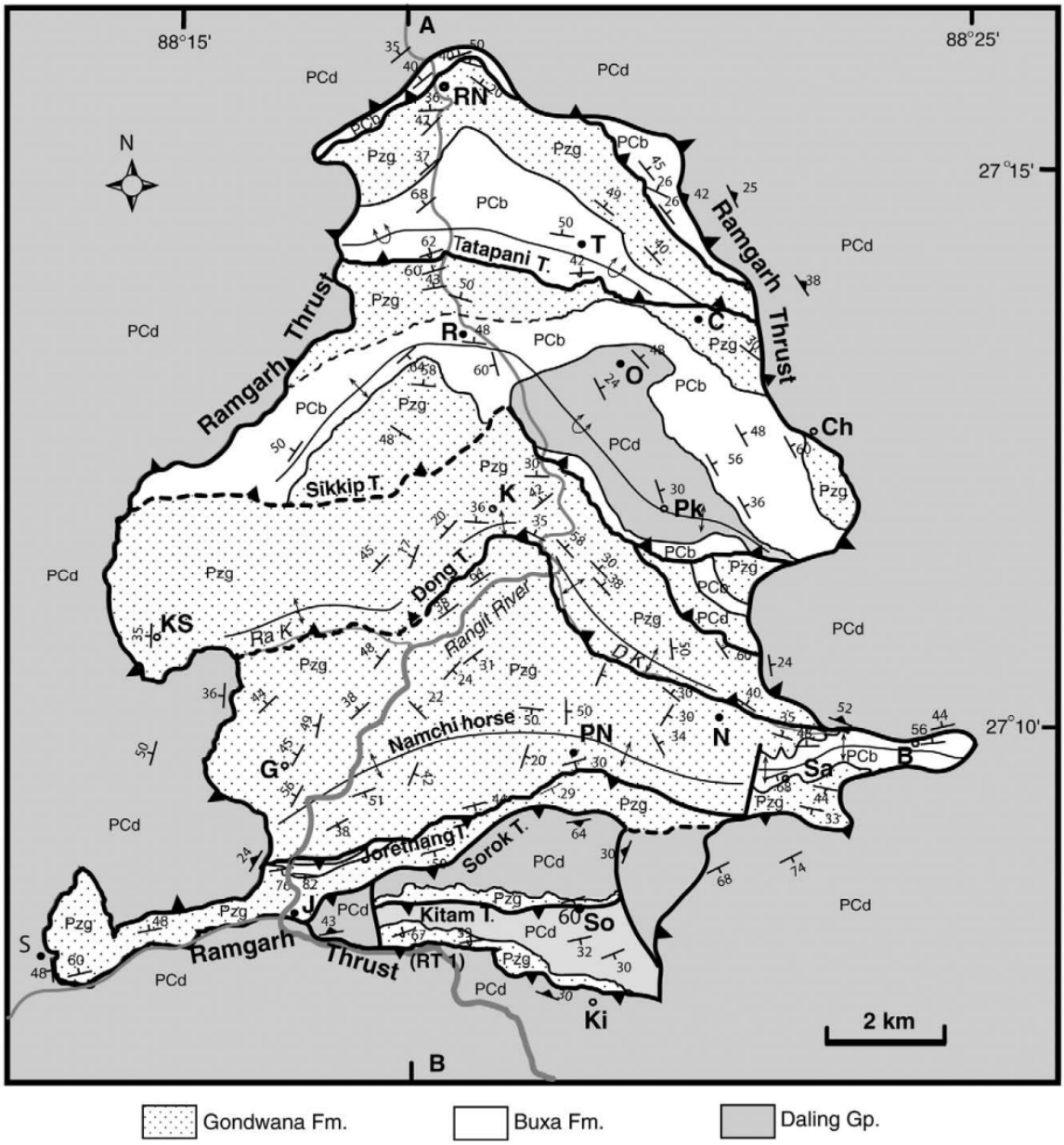

Figure 2.3. Map of the Rangit window showing the thrust slices constituting the Rangit duplex, after Bhattacharyya and Mitra, 2009. The upper LHS is repeated along horses at least eight times within the duplex. The Ramgarh thrust is the roof thrust. Towns are B—Banzyang, C—Chamchey, Ch—Chiyadaara, G—Gelling, J—Jorethang, K—Kamling, Ki—Kitam, KS—Khani Sabang, N—Namchi; O—Omchu, Pk—Pakzer, PN—Purana Namchi, R—Reshi, RN—Rangitnagar power station, S—Singrep, Sa—Samdong, So—Sorok, and T—Tinkitam. Small streams shown are RaK: Rathong Khola, DK: Dong Khola AB represents the line of cross section (Figure 2.4).

2.1.1. Main Frontal Thrust

The Main Frontal Thrust (MFT) defines the toe of the Sikkim Himalayas to the south, separating the Siwaliks Group and the quaternary sediments. In the study area, the MFT is located close to the MBT, and at depth they join together at a thrust plane called the Main Himalayan Thrust (Patro & Harinarayana, 2009; Mukul 2000).

2.1.2. Siwalik Formation

The Sub-Himalayan strata, particularly the Siwalik Formation, are the youngest of the selected units, with a Tertiary depositional age. It is structurally defined to the south by the MFT and to the north by the MBT. The unit varies from 4 – 6 km in thickness and dips towards the north at and angle between 30 and 40 °. The sedimentary section shows a consistent coarsening upwards sequence. The lower portion of the unit is largely silts and clay, which coarsens to fluvial siltstone and sandstones and eventually to sandstones and gravelly braided river deposits (McQuarrie et al. 2008). The origin of the sediments came from alluvial processes of the Himalayas through the mid-Miocene-Pliocene (Najman 2006).

2.1.3. Main Boundary Thrust

The Main Boundary Thrust (MBT) separates the Silwailks Formation from the LHS as the sediments from the Gondwana Formation of LHS have been thrust from the north, southward overtop of the Sub-Himalayan (Mukul, 2000). The thrust is present across the entire front of the Himalayas, which it parallels. It dips towards the north and is marked by a narrow zone of cataclastic rock (Hodges, K.V., 2000). The total

displacement of the MBT cannot be calculated, as there are no matching rock units in the hanging wall or footwall (Hodges, K.V., 2000) although some researchers attended to do so applying the concept of N-S balanced cross sections (McQuarrie et al., 2008; Bhattacharyya and Mitra 2009) (Figure 2.4).

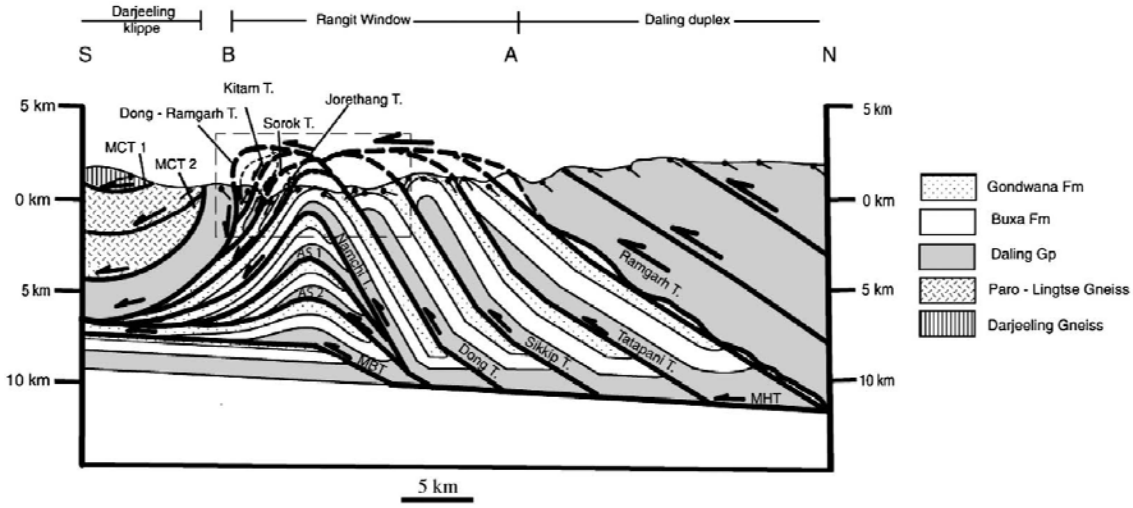

Figure 2.4. Balanced cross section of the Rangit duplex along AB (Fig. 2.3). The floor thrust of the duplex is the Main Himalayan thrust (MHT). After Bhattacharyya and MItra 2009.

2.1.4. Lesser Himalayan Sequence

The Lesser Himalayan Sequence overlies the Siwalik Formation, separated by the north-dipping MBT to the south and the Main Central thrust (MCT) to the north, and can be divided into three subunits; The Daling Group, Buxa Formation, and the Gondwana Formation. The Daling Group has a basal unit composed of a greenish white to tan quartzite Its depositional age has been dated between 1.86 – 1.83 Ga using detrial ziron ages from similar correlated lithological units (DeCelles et al., 2001 in Nepal to the west, McQuarrie et al, 2008 in Bhutan to the east). It has continuous planar bedding, which can be thickly bedded, fine-grained and interbeded with phyllite or schist (McQuarrie et al. 2008). Overlying this is a greenish grey chloritic to sericitic schist and slate dominated unit. The schist shows irregular and scaly foliations and often contains quartz veins and

blobs (McQuarrie et al. 2008). This entire unit has a variable thickness across the Sikkim Himalayas, but in the RW it is ~5 km thick with ~1.2 km of the unit exposed (Bhattacharyya & Mitra, 2009). Within the RW, chloritic slates are exposed in grey, purple and black shades, with individual beds measuring 1-2 cm in thickness and Amphibolite sills and dikes present (Bhattacharyya & Mitra, 2009). Note that the observations made by McQuarrie et al 2008 have been made in Eastern Bhutan and are assumed to be consistent in the Sikkim Himalaya.

The Buxa Formation structurally overlies the Daling Group and is a carbonate rich unit. It is composed of calcareous slates and conglomerates near the bottom (ranging in colour from bright green, to pink, to yellowish white), and bluish grey dolomites towards the top. The slates are intercalated with limestone of pink and yellowish colors, which makes them distinguishable from the Daling Group. Locally, dolomite can be intercalated as well, but with a grey quartzite interbedded. The thickness of the Buxa Formation is variable, as it has been calculated to be ~1.2 km by Bhattacharyya & Mitra (2009) with a minimum thickness of 2.5 km, calculated by McQuarrie et al. (2008). Based on detrial zircon ages from Bhutan, this unit has a maximum depositional age from the Cambrian period (McQuarrie et al. 2008)

The youngest lithological unit of the LHS is the Gondwana Formation (GF) that lies structurally above the Buxa Group. This unit / Gondwana Formation contains different lithologies and is widely exposed in the RW, with a thickness of ~1 km. Its base is made up of a basal conglomeratic horizon, which varies in matrix composition from calcareous on the bottom to argillaceous at the top. In the middle is a gritty medium-grained bluish grey sandstone and orthoquartzite with a thickness of ~20 cm. Black coal

bearing carbonaceous slate with 1-2 cm thick beds completes the sequence, showing a fining upwards trend. Paleontological evidence (Joshi, 1989; 1995; Lakshminarayana, 1995) indicates a Permian (~300 – 250 Ma) depositional age of the Gondwana Formation.

2.1.5. Ramgarh Thrust

The Ramgarh Thrust (RT) is a large thrust plane that occurs in Northern India and across the whole of Nepal. It placed the older units of the LHS above younger units, creating a duplex (Lesser Himalayan duplex, Fig. 2.4), and displacing material ~120 km southward in Nepal (Pearson and Decelles, 2005). In the Sikkim Himalaya the RT is responsible for ~125 km of minimum shortening occurring in the Rangit duplex of the Rangit Window (Figure 2.4) The RT is the roof thrust of the Rangit Window that was studied and lies north of the MBT and south of the MCT, separating the two.

2.1.6. Main Central Thrust

The Main Central Thrust (MCT) is the oldest major shear zone in the Himalayas. It marks the boundary of the highly metamorphosed GHS from the lower-grade LHS (Hodges, K.V., 2000). it has a general NW-SE trend in which it is much more irregular in its trace then the other structures. The irregular nature of the thrust plane is caused by both NW-SE and N-S trending open upright folds, erosion of which has created tectonic windows (Figure 1) revealing LHS throughout the Himalayan front. In Sikkim the MCT has been devided into two planes, MCT 1 and MCT 2 (Catlos et al., 2004; Bhattacharyya et al., 2009), defining a broad shear zone, ranging from several hundreds of metres to

several kilometers in thickness (Hodges, K.V., 2000). These planes define the roof of the Sikkim window within the study area.

2.1.7. Greater Himalayan Sequence

According to Hodges (2000), the Greater Himalaya sequence (GHS) is a lithotectonic unit that is defined by the STDS to the north and MCT to the south. In the eastern Himalaya the GHS varies in width from 60-100 km. The GHS is composed of orthogneiss, paragneiss, schist, quartzite, occasion exposures of marble and amphibolite layers, and Miocene leucogranites. The base of the unit is largely biotite-muscovite gneiss of middle to upper-amphibolite facies with migmatic leucosomes present as you migrate up section occurring in various scales from centimetre-sized dikes to kilometre-sized plutons. Close to the top of the sequence, is augen orthogneiss with few metasedimentary intercalations. The age of the unit is still not well determined, but using detrital zircons and Rb-Sr studies an estimated Cambrian-Ordovician age has been determined. Note that many of these granite gneisses are now dated as Cambrian-Ordovician by Cawood et al. (2007) as well.

2.1.8. Southern Tibetan Detachment

The South Tibetan Detachment system (STD) is a system of low-angle ductile shear zones and brittle faults with a normal sense of movement (Kellett et al., 2009). It is the structure that separates the GHS from the overlying northern Tethyan Himalaya, which were thrusted above from 26 Ma until ~15.5 Ma (Kellet et al., 2009) during the movement of the STD. In the footwall is the highly metamorphosed GHS and in the

hanging wall are the Tethyan sediments. The ductile shear zone is made up of two branches (M. P. Searle et al., 2006), which converge towards the north that create a single large high strain zone (M. P. Searle et al., 2006, Hollister and Grujic 2006, Kellett et al 2009).

2.1.9. Tethys sedimentary sequence

The Tethys sedimentary sequence consists of a 13 km thick and nearly continuous lower Paleozoic to lower Tertiary marine sedimentary succession (Liu and Einsele, 1994). The unit spans across the Himalayas for over 1500 km, from NW India, across Nepal, and into Bhutan (Fig 1.). It is an extensive unit that outcrops in the west and eastern portions of the Himalayas, with limited exposures within the central section. Liu and Einsele (1994) describe the base of the Tethys consisting of various metamorphic schists, phyllites, quartzite's, marbles and gneisses. Overlying the basement is a common alternating sequence of limestone and fine to medium-grained sandstone that occurs into the Upper Triassic. Capping the sequence is a transition from black shale and siltstone to marl and massive limestone interbedded with sandstone and topped with conglomeratic sandstone, ending in the Pliocene.

2.2. Transverse Antiforms

Through the mechanisms of continental collision, material is folded and deformed as it is responding to the compression. In the Himalayas, the direction of crustal shortening is north – south, as the Indian plate is being driven into the Eurasian. This would result in folding with fold axes trending perpendicular to direction of the

maximum compression. However, there are structures that display a transverse north-south trend, contradictory to conventional thought. The major Himalayan rivers run transverse to the primary geologic structures from the edge of the Tibetan Plateau and perpendicular to the orientation of the range (Montgomery and Stolar, 2006). Approximately at the same locations as these rivers are large-scale transverse structures that perhaps show a correlation between river incision and focused deformation. These features can also be observed through tectonic windows and half windows, which are created through erosion along a thrusting hanging wall.

Normally an antecedent river, predating the development of the geologic structure, takes the path of least resistance, where it can easily incise and drain efficiently creating a pathway, without the creation of large-scale geological structures (Montgomery and Stolar, 2006). For a consequent river, postdating the geologic structures, it would also follow the least resistant path, yet it would follow structural lows, not structural highs such as along anticlines. In the case of the Rangit Window, the Rangit River runs through the LHS that is exposed from erosion in the anticlinal core. This contradicts typical conceptions of river paths, with the idea of unloading material at the surface through river incision, which may inhibit the development of Himalayan river anticlines and create an increase in exhumation rates (Simpson, 2004). However there are indications of the concomitant incision and localized fold amplification.

2.3. Tectonic Windows

Within the state of Sikkim, India, a double tectonic window has been formed. Located in the centre of the state, two major southward flowing rivers, the Tista and its

tributary the Rangit, have created this window through erosion. The outer half window is bound entirely by the MCT but does not display a closed outcrop pattern as the southern portion has been eroded away (Bhattacharyya & Mitra, 2009), resulting in a mushroom shaped window known as the Tista window (Figure 2.2). Within this half window lies the second window, which is completely bound on all sides by the MBT at the base and the RT in the roof, called the Rangit window (Figure 2.3). This feature is the main focus of this project, as it exposes outcrops of the Gondwana Formation and micaceous sandstones associated from the core of the Rangit window. As the Rangit River flows through the core of the window, it suggests the idea that perhaps the river is aiding in the development of this feature.

CHAPTER 3 METHODOLOGY

3.1. Introduction to $^{40}Ar/^{39}Ar$ Dating.

The $^{40}Ar/^{39}Ar$ method of dating was developed in 1966 by Merrihue and Turner (in Dickin, 2005). A standard dating method at that time was K-Ar dating, which measured the concentrations of both potassium and argon, which had limitations. The ages that were calculated from this technique, at times, yielded dates that were too old due to the presence of excess radiogenic ^{40}Ar in the sample. This can occur through physical contamination from older material or incorporated through processes other than the decay of ^{40}K (McDougall and Harrison, 1999). The $^{40}Ar/^{39}Ar$ method can sometimes overcome this constraint by measuring several isotopes of argon (^{36}Ar, ^{37}Ar, ^{39}Ar and ^{40}Ar) within the sample, eliminating the measurement of potassium altogether (Faure, 1986). The ratios of $^{40}Ar/^{36}Ar$, $^{37}Ar/^{39}Ar$, $^{36}Ar/^{39}Ar$ and $^{40}Ar/^{39}Ar$ are measured, and help constrain the age of the sample..

This dating technique does not require measurement of potassium, but requires the presence of K-bearing minerals within a sample. The presence of argon within a sample is due to the decaying process of ^{40}K. Argon is formed from positron decay and electron capture, two different processes of nuclear radioactive decay of ^{40}K (McDougall and Harrison, 1999).

3.2. Radioactive Decay

The original ^{40}K, the parent isotope, is unstable and because of the decaying process of either electron capture, or positron emission, it undergoes dual-decay to stable

daughter ^{40}Ar (~11% of decay) and ^{40}Ca (~89% of decay) by beta emission (McDougall and Harrison, 1999). For the ^{40}Ar/^{39}Ar dating technique, the decay scheme of ^{40}Ca is ignored. The radioactive decay that potassium is experiencing has the half life of 1.25 billion years, which denotes the time it takes for one half of the parent atoms to decay into daughter atoms. The rate at which radioactive nuclear decay occurs is proportional to the number of parent atoms remaining in the system (Faure and Mensing, 2005). This is expressed as a decay constant. The buildup of radiogenic argon can be expressed as a reaction in eq. (1) (McDougall and Harrison, 1999):

$$^{40}\mathrm{Ar}^{*} = \frac{\lambda_e}{\lambda} {}^{40}\mathrm{K}(e^{\lambda t} - 1) \qquad \text{(Eq. 1)}$$

where ^{40}Ar* represents the number of ^{40}Ar atoms after time t, ^{40}K represents the number of 40-potassium atoms, λ_e represents the decay constant of ^{40}K to ^{40}Ar, λ represents the total decay constant of ^{40}K, *t* represents time and e is the logarithm to the base e.

The formation of ^{39}Ar however is more complicated, as it needs to be produced artificially. This is accomplished in a nuclear reactor by the bombardment of the ^{39}K nucleus in the sample by fast neutrons, which results in ^{39}Ar through the process of transmutation (McDougall and Harrison, 1999), transforming one element into another by the means of nuclear reactions (eq. 2). The reaction can be described as:

$$^{39}_{19}\mathrm{K} + ^{1}_{0}\mathrm{n} = ^{39}_{18}\mathrm{Ar} + ^{1}_{1}\mathrm{H} + Q \qquad \text{(Eq. 2)}$$

where superscript represents the atomic weight of the each element, subscripts represents the atomic number, *n* represents a neutron, and *Q* represents the energy released or absorbed in the reaction (McDougall and Harrison, 1999). The amount of ^{39}Ar produced from the reaction depends on length of the irradiation, the neutron flux density and the amount of neutron capture, which is expressed as *J*, the irradiation parameter (eq. 3) (McDougall and Harrison, 1999). These parameters are difficult to determine independently, therefore a mineral standard, or monitor, of a known age is irradiated with the sample of unknown age. The J-value for the monitor can then be used to determine J for the sample (Faure and Mensing, 2005). The former can be calculated using the following equation:

$$J = \frac{e^{\lambda t_m} - 1}{^{40}Ar^*/^{39}Ar} \qquad \text{(Eq. 3)}$$

where *J* is the irradiation parameter, ^{40}Ar*/^{39}Ar represents the ratio in the monitor, t_m represents the age of the flux monitor, and λ represents the total decay constant of ^{40}K. The half-life of ^{39}Ar is relatively short, 269 years, and quickly decays back to ^{39}K. This can be ignored as samples are usually analyzed within a few months of irradiation, and the amount of decay is negligible.

3.3. ^{40}Ar/^{39}Ar Dating Method

The ^{40}Ar/^{39}Ar dating method measures the ratio of four argon isotopes: ^{36}Ar, ^{37}Ar, ^{39}Ar, and ^{40}Ar (Dickin, 2005). The isotopes are degassed from the sample and released where they are measured with a high-sensitivity mass spectrometer. Common degassing

techniques involve the use of lasers and furnaces (Figure 3.1). The two main types of lasers that are used are infrared (IR) and ultraviolet (UV). These extraction techniques will be discussed in more detail in 3.3.3.

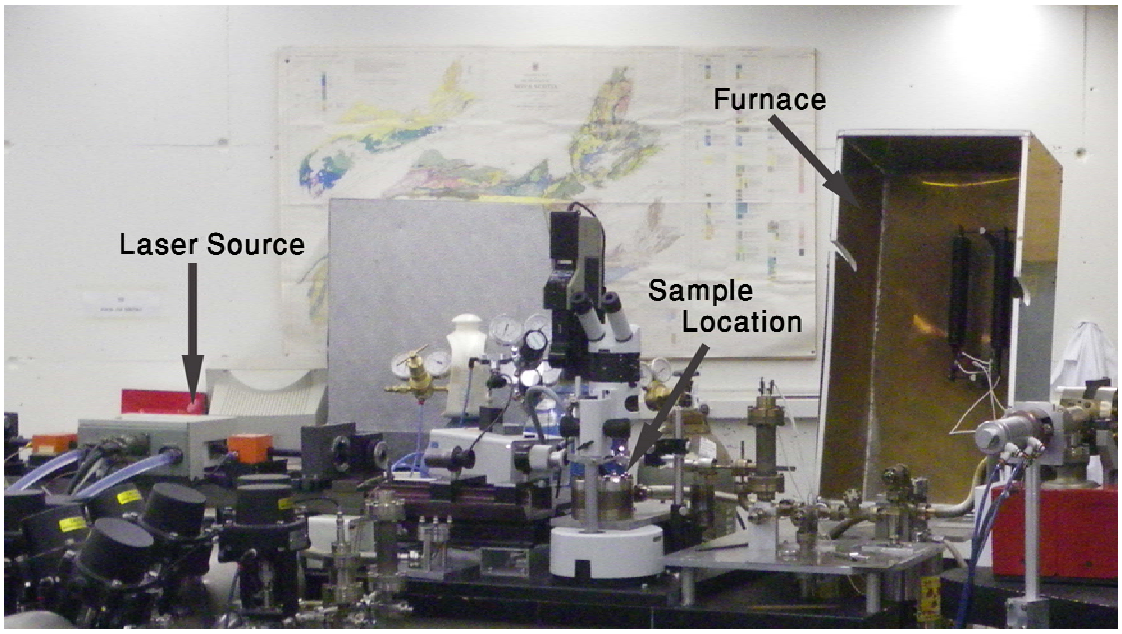

Figure 3.1. Quantronix 117 Nd:YAG laser and double-vacuum furnace located in the Argon Isotope laboratory at Dalhousie University.

3.3.1. Mass Spectroscopy

The degassed argon isotopes travel through the sample line to a high-sensitivity mass spectrometer where they are measured. They are collected and become positively charged by an ionizer. A magnetic analyzer is used to independently deflect each isotope along a curved track to the analyzer, as each isotope has a different atomic mass. The heavier the ion, the less tendency it will have to curve, and the lighter ions will have a greater tendency to be curved. The mass spectrometer is attached to a detector where the ion beams are measured and the abundance of argon isotopes in the sample recorded. Once the isotopes are measured, the ratios of $^{40}Ar/^{39}Ar$ and $^{36}Ar/^{39}Ar$ can be determined. Figure 3-2 shows the different components of a mass spectrometer.

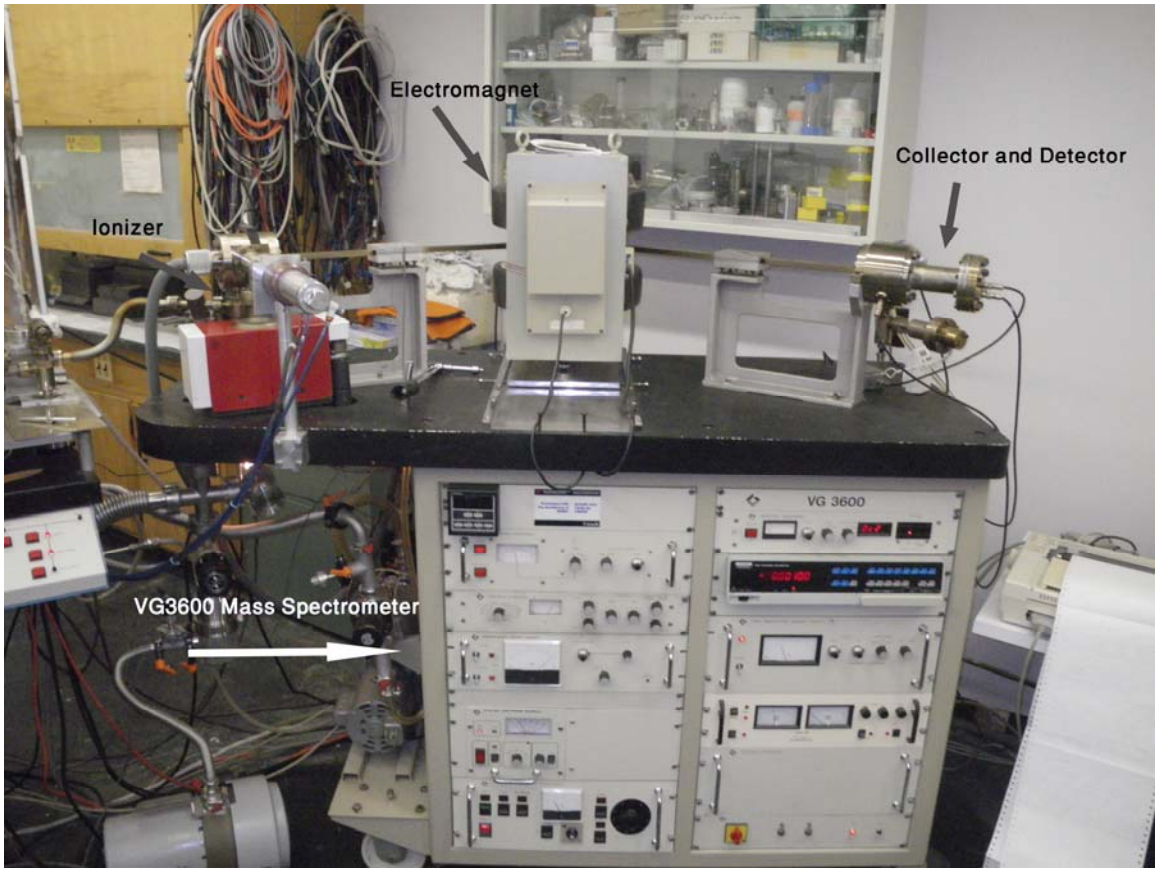

Figure 3.2. VG3600 Mass Spectrometer showing the ionizer, electromagnet, and collector and detector locations, located in the Argon Isotope laboratory at Dalhousie University

3.3.2. Age Equation

The measurement of ^{36}Ar is always made to infer the amount of atmospheric ^{40}Ar in the sample. The ratio of $^{40}Ar/^{36}Ar$ is 295.5 for atmospheric argon; therefore the amount of atmospheric ^{40}Ar in the sample is 295.5 times the amount of ^{36}Ar. To measure the amount of radiogenic $^{40}Ar^*$ produced from a sample, the total amount of ^{40}Ar measured is corrected by subtracting the atmospheric component. The above ratios are the basis of the dating method, as they indicate the amount of decay that has occurred through time and thus the age of the sample. The age equation (eq. 4) can be used to determine the age based on the ratio of the isotopes (McDougall and Harrison, 1999) expressed as:

$$t = \frac{1}{\lambda} \ln\left(1 + J \frac{^{40}\mathrm{Ar}}{^{39}\mathrm{Ar}}\right) \qquad \text{(Eq. 4)}$$

where t represents the age of the sample, λ is the decay constant, ln is the natural logarithm, J is the irradiation parameter, ^{40}Ar is the argon produced by *in situ* radioactive decay and ^{39}Ar is the argon produced by the irradiation of ^{39}K within the sample.

3.3.3. Closure Temperature

By using the equation 4, the age calculated is strictly based on the number of parent and daughter atoms present at the time of sampling. This may not necessarily provide a crystallization age of a sample, depending on its thermal history. The closure temperature represents a time in which the mineral has cooled past a temperature where there is no longer solid-state diffusion of ions from the crystal. If the crystallization temperature were lower than the closure temperature of a mineral, then the age that would be calculated would refer to the crystallization age. Also if the crystallization temperature were higher then the closure temperature, then one would obtain the cooling age. If there were thermal resetting of previously crystallized and cooled minerals, like detrital minerals, then again, one would obtain cooling age and not the heating age. If an existing mineral is below its closure temperature, accumulating argon, and is subjected to enough heat to reheat the sample above its closure temperature then the mineral would be completely reset, losing all of the accumulated argon, resulting in the loss of earlier thermal history. Events such as magmatism, rifting, faulting and metamorphism are all examples of how thermal resetting can occur (McDougall and Harrison, 1999).

Each mineral has a different closure temperature for different isotopic systems, which depends largely on the activation energy for diffusion but also on the size of the sample grain (radius) and the cooling rate (Harrison et al., 2009). The closure temperature increases with both increasing cooling rate and increasing grain size, shown in Figure 3.3 for muscovite. This can be expressed in the Dodson equation (eq. 5) (Faure and Mensing, 2005):

$$T_C = \frac{E/R}{\ln[(ART_C^2 D_0/a^2)/(E\,dT/dt)]} \qquad \text{(Eq. 5)}$$

where T_C represents the closure temperature, E represents the activation energy, R represents the gas constant, A represents a geometry factor (55 for diffusion from a sphere and 27 from a cylinder), D_0 represents the frequency factor, a represents effecive diffusion radius. The concept of studying the thermal history of rocks, based on closure temperature ages, is referred to as thermochronology (McDougall and Harrison, 1999).

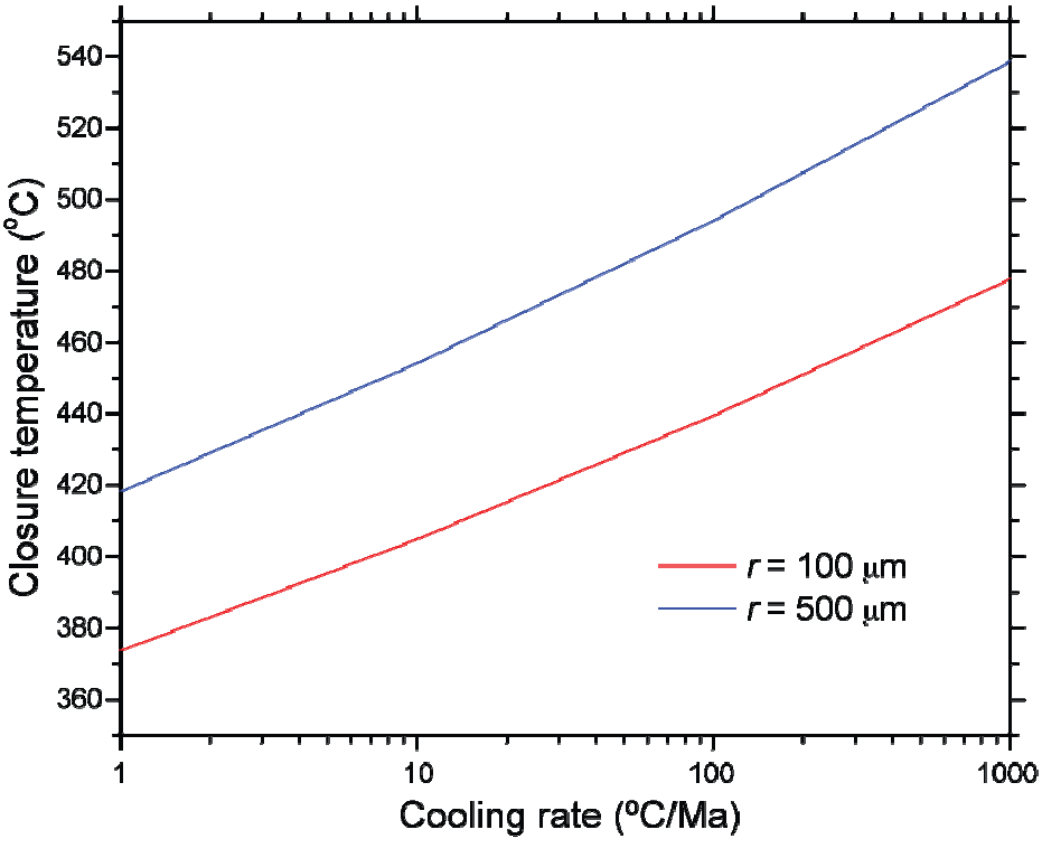

Figure 3.3. Variation of Tc of muscovite with cooling rate and diffusion dimension for Arrhenius parameters appropriate to 5kbar pressure (E = 64 kcal/mol and Do = 20 cm2/s). After Harrison et al., 2009.

3.3.4. Muscovite

Appropriate minerals that can be used in this method contain potassium within their crystal lattice. Many minerals and rocks can be used for analysis, such as: feldspars, feldspathoids, mica, amphibole, pyroxene, whole rock, volcanic glass, evaporites, and manganese oxides (McDougall and Harrison 1999).

Muscovite has an ideal composition for $^{40}Ar/^{39}Ar$ dating of $K_2Al_4Si_6Al_2O_{20}(OH,F)_4$, which allows a maximum total amount of 9.7% potassium to be incorporated within its structure (McDougall and Harrison, 1999). It is also found widely in granitic plutons, metamorphic rocks and detrital grains in sedimentary packages, which gives it a wide range of application as a dating mineral. For muscovite, the closure

temperature has been calculated to be ~425°C (Harrison et al., 2009) (Figure 3.3). This value is determined using an *r*-value of 500 μm from figure 3.3, and a cooling rate of 1.5 °C/Ma. However if an *r*-value of 100 μm is substituted in for 500 and the cooling rate is the same, then a closure temperature of muscovite is ~380°C. It can vary greatly according to grain size and cooling rate.

3.4. Dalhousie Argon Isotope lab

The Argon Isotope lab run by Keith Taylor at Dalhousie University was selected to perform the single-grain total fusion $^{40}Ar/^{39}Ar$ dating technique used in this thesis. The facilities available in the lab include a VG 3600 high-sensitivity mass spectrometer and two argon extraction systems (Fig. 3-4).

3.4.1. Extraction Techniques

Before extraction from a sample takes place, a series of 'blank' analyses are made. A blank is a measurement to determine signal strengths in the mass spectromter at the masses corresponding to each of the measured argon isotopes before a sample is introduced into the mass spectrometer. Following each analysis, a blank correction is made to the data.

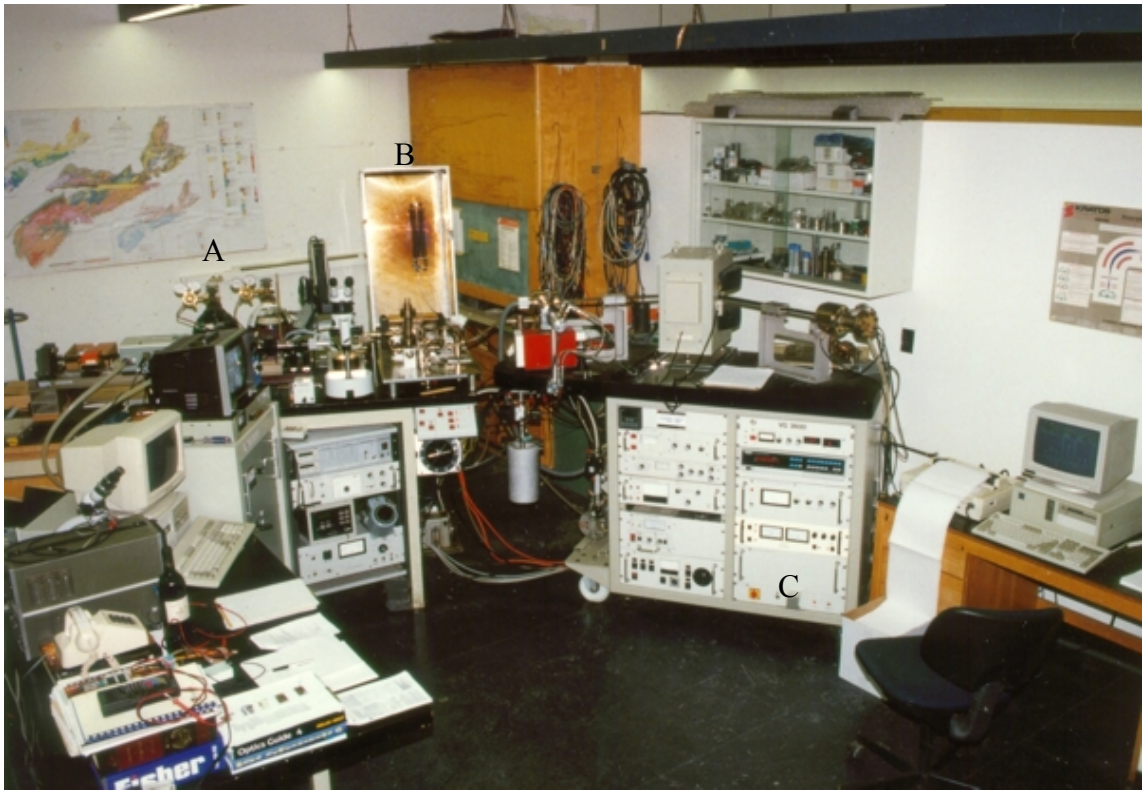

Figure 3.4 The Argon Isotope laboratory located at Dalhousie University. Letters correspond to: A - Quantronix 117 Nd:YAG laser, B – double vacuum furnace, and C – VG3600 Mass Spectrometer.

The first extraction system is an internal tantalum resistance double-vacuum furnace, which is used to carry out conventional $^{40}Ar/^{39}Ar$ step-heating analyses of separated minerals. A few hundred grains of a mineral, or a few milligrams, are placed into an aluminum capsule and sent to a nuclear reactor. Once returned from irradiation, they are then placed within the furnace apparatus and multi-grain temperature controlled out-gassing is performed. This technique generally has a relatively high blank associated with the analysis. The amount of argon produced at each step can be analyzed isotopically and a succession of apparent ages can be determined (McDougall and Harrison, 1999). If the sample has retained its radiogenic argon since passing through its closure temperature, then the proportions of ^{40}Ar and ^{39}Ar will be the same throughout

the heating process. Once the argon isotopes are measured by the mass spectrometer, a graphical plot is made, displaying the ages associated with the amount of ^{39}Ar released, called an age spectrum (Fig. 3-5).

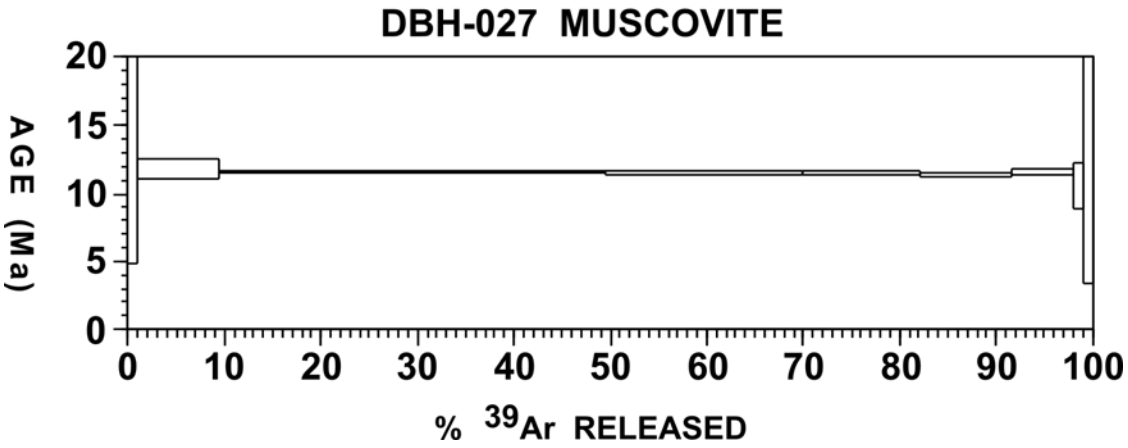

Figure 3.5. Age spectrum of a Bhutan sample, DBH-027, obtained by Dawn Kellet.

The second extraction system uses a laserprobe applying a Quantronix 117 Nd-YAG laser that can be used at either IR or UV wavelengths. This system analyses single mineral grains by the means of total fusion or traverse intragrain analysis. The UV laser is used to perform traverse intragrain analysis. This technique uses the fine focus of the UV laser to create ablation pits (~50 – 100 μm) (Fig. 3-6) across a single grain. The laser is focused on a single spot along the face of a mineral and creates a small hole allowing a small amount of gas to be released and measured. This is done for a series of spots along the mineral and allows the comparison of argon contained within different localities of the grain. Ages are calculated from these spots and this can identify if the grain has experienced substantial heating through its history partially resetting the grain. Ages that are similar to one and other indicate that the grain has a uniform age and any heating events have not been large enough to disrupt the grain. Ages that vary slightly from each

other, along the traverse, indicate that a portion of the grain has been affected by a heating event.

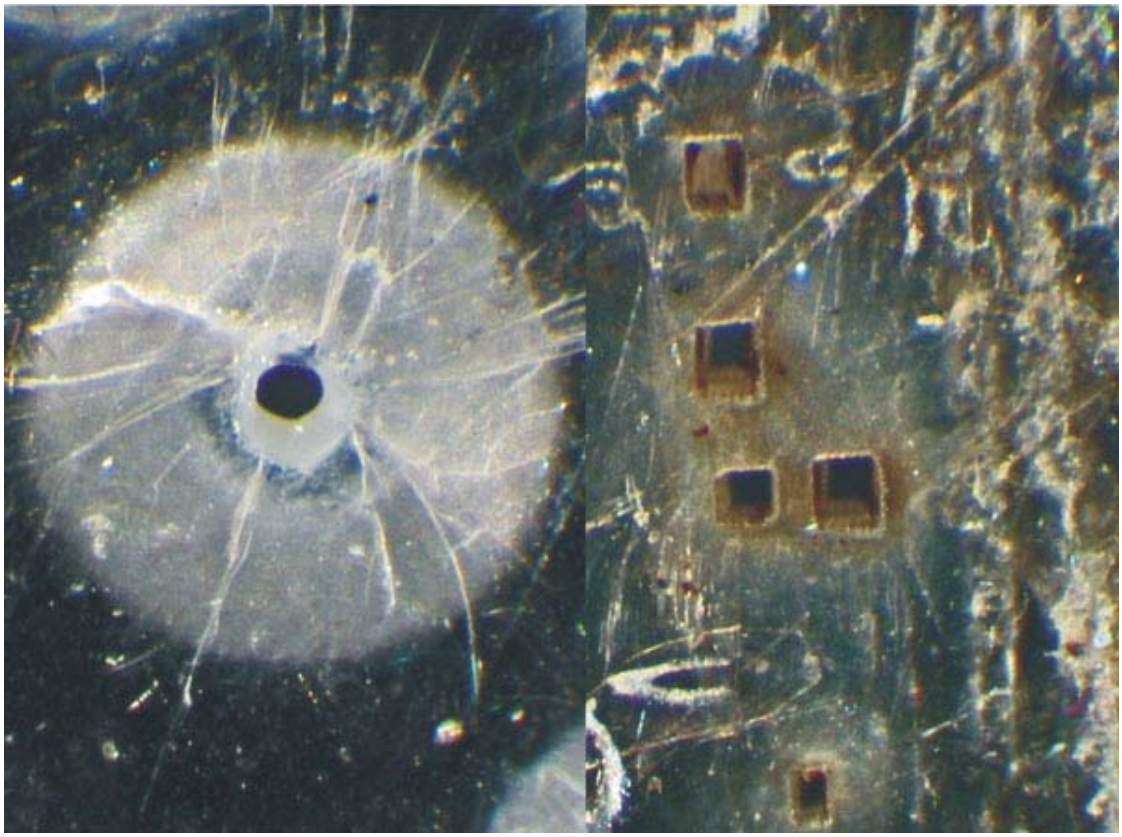

Figure 3.6. Image of a single muscovite grain showing on the left a spot made with IR laser, and on the right ones made with the UV laser. The largest UV spots near the centre have side lengths ~150 m and depths ~400 m; scale is the same across whole image. Note large halo surrounding central hot zone in the IR image.

The technique used in this thesis is the total fusion of a single grain, which is performed by the IR laser. It extracts the total amount of gas and results in a single age. Single grains were used for this analysis. Once the grains are mounted and returned from irradiation, the IR laser is then used to focused to the approximate size of a sample grain (~<100 μm) and the intensity of the laser is increased until the grain is completely thermally degassed. The evicted gasses are then measured with the mass spectrometer and an age is calculated based on the observed $^{40}Ar/^{39}Ar$ ratio. Once all of the single

grains from a sample have been measured a cumulative probability plot is created displaying the frequency of age ranges and a cumulative curve showing the peaks of ages (e.g. see Results).

3.5. Sample Preparation of Detrital Muscovite

Before analysis, the selected samples must be separated, prepared one at a time, and one must ensure that the laboratory and instruments are clean, to prevent any contamination between samples. The hand samples are cleaned of any type of surficial debris such as vegetation and soil that could potentially cause contamination, using a steel brush. The sample is then broken down using a jaw crusher, unless it is too large in which case a sledgehammer is used to break it down into smaller pieces that then can be crushed. From the jaw crusher, the size fractions of the sample are between gravel and pebble sized, and must be further broken down. Using a milling machine, the remaining pieces of the sample are crushed into a fine-to-coarse grained powder, and are then washed. Using a continuous slow flow of water, the powder is rinsed resulting in a cloudy liquid, and the process continues until the water clears of any cloudiness. When this is complete, the sample powder is then dried in an oven at a low temperature until all moisture has been evaporated. In some cases the first step is sufficient to liberate the mica with the milling, however the mica can be broken and there is a need for as less damaged grains as possible (intact grains are needed) because the age may depend on the grain size or there may be different populations (generations) of the same mineral species which may be separated according to their mean grain size.

After the sample was dried in the oven, it was ready for mineral picking. Using a binocular microscope, a fine-tipped paintbrush and a small glass vial, 50 muscovite grains >~250 μm were hand selected for each sample. By moistening the tip of the paintbrush and viewing through the microscope, grains were carefully obtained by making contact with the tip of the brush, and transferred into a vial. Grains were selected based on purity and size (McDougall and Harrison, 1999), with a focus on large, clear grains, Once each sample was complete, the vial of grains were labeled appropriately and set aside for grain mounting before analysis (Fig. 3-7).

Keith Taylor, of the Argon Isotope lab, performed a final separation of the detrital muscovite grains for mounting. Grains were separated based on size, with grains ~500 μm to 1.0 mm being mounted together and grains ~<500 μm mounted together. A single grain was also selected, >1.0 mm in size, to be used for traverse intragrain analysis. There was also an observance for grains that could possibly be contaminated or fragmented.

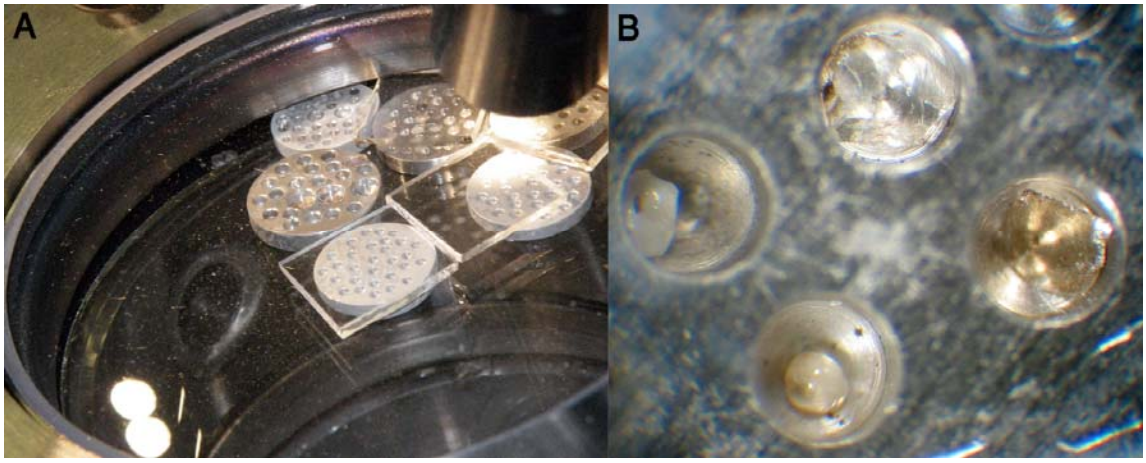

Figure 3.7. (A) Detrital muscovite grains mounted in 1 cm diameter aluminum disks awaiting analysis. (B) Close up of the muscovite grains. The crystal in the upper most drilled hole is still intact, while the lower most hole contains a degassed muscovite remnance.

3.6. Single Grain Total Fusion Analysis

Note that for this thesis, Keith Taylor supervised and performed the complete analysis on the detrital muscovite grains.

The separated mica grains were placed in holes drilled in 1 //cm diameter Al disks, which were stacked in an aluminium irradiation canister. Interspersed among the samples were five to seven aliquots of the flux monitor, Fish Canyon tuff sanidine, which has an apparent K-Ar age of 28.205 ± 0.046 Ma (Kuiper et al. 2008). The canister was irradiated with fast neutrons in the nuclear reactor at McMaster University in Hamilton, Ontario, Canada. At the Argon Isotope Lab at Dalhousie University, the Quantronix 117 Nd:YAG laser with a wavelength of 1064 nm operated in continuous mode was used to carry out total fusion analyses of each of the grains. Isotopic analyses were made in a VG3600 mass spectrometer using an electron multiplier collector to measure the $^{40}Ar/^{39}Ar$ and $^{36}Ar/^{39}Ar$ ratios. Errors are reported at the 2σ level and include the uncertainty in the irradiation parameter, *J*, but do not incorporate uncertainty in the assumed age of the flux monitor.

CHAPTER 4 RESULTS

4.1. Sample Descriptions

Note that only three thin sections were made (SK036, SK038 and ISIK0837) from the five samples obtained (SK036, SK038, ISIK0805, ISIK0836 and ISIK0837); as well, only two hand samples remain (ISIK0837 and ISIK0836). This was due to the focus of obtaining detrital grains from each sample, and the size of samples selected limited the availability of thin sections to be made.

4.1.1. Hand Samples

4.1.1.1. ISIK0836

The sample ISIK0836 is a heavily oxidized chestnut brown to orange colour, with occasional grey patches. It is medium-grained, showing slightly finer material than in ISIK0837. There is no appearance of bedding or sedimentary structures, but an S_1 slatey cleavage can be weakly observed. Individual micas can be observed throughout the sample, randomly dispersed with no clear indication of alignment. They are finer grained than in ISIK0837, ~0.5 mm in size, and seem to compose more of the sample.

4.1.1.2. ISIK0837

The sample ISIK0837 is bluish-grey in colour along fresh faces and oxidized to an earthy orange-brown on exposed sides. It is medium to coarse-grained with no appearance of relict bedding, cleavage or any sedimentary features. Individual micas can

be observed throughout the sample, as their luster is evident in the light. They can be measured at ~1 mm in size. Along the freshly cut face of the sample a weak mineral lineation can be observed by the alignment of mica, with the trend of the long axis of the grains being in the same general direction.

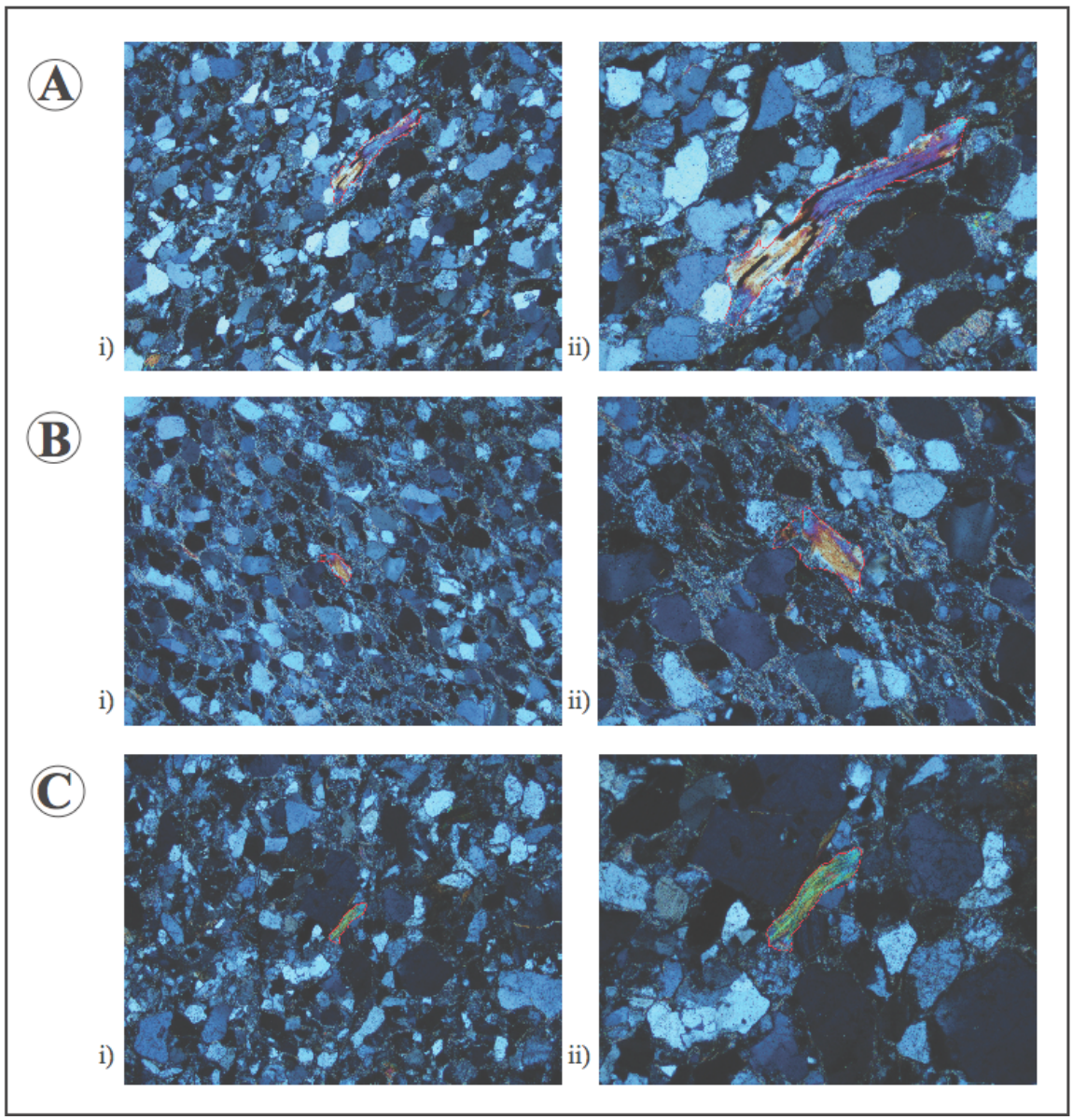

Figure 4.1. Shown are the thin sections of the available samples. Outlined in red are detrital muscovite grains found in each sample. The preferred general orientation of grains can be observed as well. A i) SK038 at 6.25 mm F.O.V ii) 2.5 mm F.O.V. B i) SK36 at 6.25 mm F.O.V. ii) 2.5 mm F.O.V. and C i) ISIK0837 at 6.25 mm F.O.V. ii) 2.5 mm F.O.V. Note F.O.V = field of view.

4.1.2. Petrological Descriptions

4.1.2.1. ISIK0837

The sample ISIK0837 (Fig. 4.1c) was poorly sorted, with no indication of bedding or grading of the sediment. The rock was composed of detrital grains that were inequigranular, with variable grain size from 0.1 mm – 4 mm and sub-angular to rounded in shape. The composition of the rock consists of quartz (70%), plagioclase (10%), lithic fragments (5%), biotite (5%), k-feldspar (2%), muscovite (2%), opaque grains (1%) and a sericite matrix (10%). The quartz grains show subgrains in the majority of grains observed, which also display undulose extinction. The grains were 0.5 mm – 1.5 mm in size and ranged between sub-angular to well rounded in shape. The plagioclase grains displayed polysynthetic twinning that had been displaying discontinuous tapering twins in grains. The grains ranged in size from <0.5 mm to 4 mm and were sub-angular in shape. The lithic fragments consisted of very fine-grained sandstone as small quartz grains could be observed within the clasts. They were rounded in shape and ~0.5mm – 1mm in size. The biotite grains showed pleochroism in PPL, changing form light brown to a medium brown. The grains were sub-rounded and were ~0.5 mm in size. The K-feldspar grains displayed weak tartan twinning in a few grains, as well as perthitic exsolution and were interpreted as microcline. The grains varied in size from 0.5 mm – 1 mm and were sub-angular to sub-rounded in shape. The size of muscovite was from 0.5 mm – 1.5 mm in length. The matrix consisted of very fine-grained muscovite / sericite, which appeared fibrous and was a secondary mineral, occurring as a product of metamorphism. The muscovite grains based on their size relative to the sample and

shape; were determined to be detrital grains. S_1 schistosity / slaty cleavage could be observed in the sample, as a weak alignment of the muscovite from the matrix, as well the weak general preferred orientation of the long axis of the detrital mineral grains and lithic clasts.

4.1.2.2. SK036

The sample SK036 (Fig. 4.1b) is moderately sorted, showing medium grained, fairly equigranular grains throughout the sample with a range in size from <0.1 mm – 1.5 mm and displaying angular to rounded detrital grains of quartz, muscovite and lithic fragments. It is largely clast/grain supported, with the matrix infilling space between the grains and lithic clasts, and no indication of bedding. The rock consists of grains of quartz (75%), opaque mineral (5%), muscovite (~2%), lithic fragments (2-3%) and sericite matrix (15%). The quartz grains commonly displayed subgrains and undulose extinction. The size of the grains ranged from <0.1 mm – 1 mm and showed sub-angular to rounded shapes, with the smaller detrital grains commonly being more rounded than the larger ones. The unidentified isotropic mineral had an irregular shape, occurring as what appeared to be small blobs, yet still maintaining a crystal shape. These grains varied from angular to sub-rounded and varied in size, from 0.5 mm – 1 mm. The muscovite grains displayed lengths between 0.5 mm – 1.5 mm. Based on the relative size in comparison to the rest of the sample, and random dispersion; they are interpreted to be detrital grains. The lithic fragments were composed of sandstone, as very fine-grained quartz grains were observed within them. These fragments were sub-rounded and showed sizes between 0.5 mm and 1 mm. The matrix consisted of secondary mineralized, very

fine-grained muscovite / sericite showing fibrous sheets and high birefringence. Within the matrix, a weak S_1 planar fabric could be observed, as slatey cleavage was defined by the alignment of secondary muscovite. There was also a general weak preferred grain orientation of all the grains in the same direction of the S_1, which was apparent in most of the sample.

4.*1.2.3. SK038*

The sample SK038 (Fig. 4.1a) was similar to SK036, yet with planar fabrics that were more strongly defined. It showed low-to-moderate sorting, typically inequigranular with medium-grained fractions of quartz and lithic fragments dominant, ranging from angular to sub-rounded in shape with a size range from <0.1 mm – 2 mm The grains are clast supported with less of a matrix present than in SK036, with no indication of bedding. The rock consisted of grains of quartz (60%), lithic fragments (20%), sericite matrix (10%), plagioclase (5%), muscovite (1-2%), biotite (1%), and trace amounts of opaque and isotropic minerals. Much like the quartz grains from the previous sample, the quartz grains in this sample displayed subgrains and undulose extinction. The grains range from angular to sub-rounded in shape and range in size from <0.1 mm – 1mm. The lithic fragments display a chestnut brown colour in Plane Polarized Light (PPL) which does not change with the rotation of the stage and the colour is persistent when viewed in XN, showing very weak, low order birefringence. The fragments are too fine-grained to determine mineralogical compositions. Numerous fragments have an irregular shape and are angular to sub-rounded with a size range between 0.5 mm – 1.5 mm. The plagioclase grains display polysynthetic twinning, with some alteration observed in the twins, as they

are discontinuous in grains, and these are therefore interpreted deformation twins, not growth twins. Plagioclase grains range in shape from sub-angular to sub-rounded, and in size from <0.1 mm – 0.5 mm. Muscovite grains occur with grains ranging from 0.5 mm – 2 mm in length. They were sub-rounded in shape and interpreted to be detrial. The biotite grains appeared brown in PPL and displayed moderate pleochroism. The grains were 0.1 mm – 0.5 mm in size and were anhedral to sub-hedral in appearance. The matrix is composed of a very fine-grained muscovite / sericite. In this sample, the foliation was stronger. An S_1 planar schistosity fabric was defined by the alignment of muscovite from the matrix. There was also a general preferred orientation of the detrital grains with the long axis trending the same direction as the planar fabric.

4.1.2.4. Summary

The three thin sections, ISIK0837, SK036 and SK038, all displayed similar characteristics to one and other in appearance and the structures found within them. They were consistently dominated by detrital quartz grains and hosted by a matrix composed largely of sericite. Also found in all of the samples were detrital muscovite grains that were much larger than the sericite in the matrix. Each of the samples displayed a consistent S_1 planar fabric, which was weak in SK36, but still present, showing slatey cleavage with the alignment of sericite (secondary muscovite) from the matrix. These samples have been classified as the same type of rock. It is a metamorphic sedimentary rock that does not display slate characteristics, nor does it display schist properties. Based on this, it has been classified as a quartz psammite.

4.2. $^{39}Ar/^{40}Ar$ Single Grain Total Fusion Data

From each sample 16-28 largest muscovite grains have been analyzed (N=119). The number of grains varies as they were separated by size. The remaining muscovite grains from each sample are smaller and the mass spectrometer operation conditions were not suitable for precise measurements during the thesis. The remaining samples will be measured, as soon the operating conditions are suitable.

The muscovite single grain IR laser total fusion $^{40}Ar/^{39}Ar$ age data are given in age probability histograms and in Table 1. The age distributions are plotted for all the grains together (Figure 4.2) and for the each sample (Figure 4.3). The table of the IR laser single –grain muscovite argon summary can be found in Appendix A.

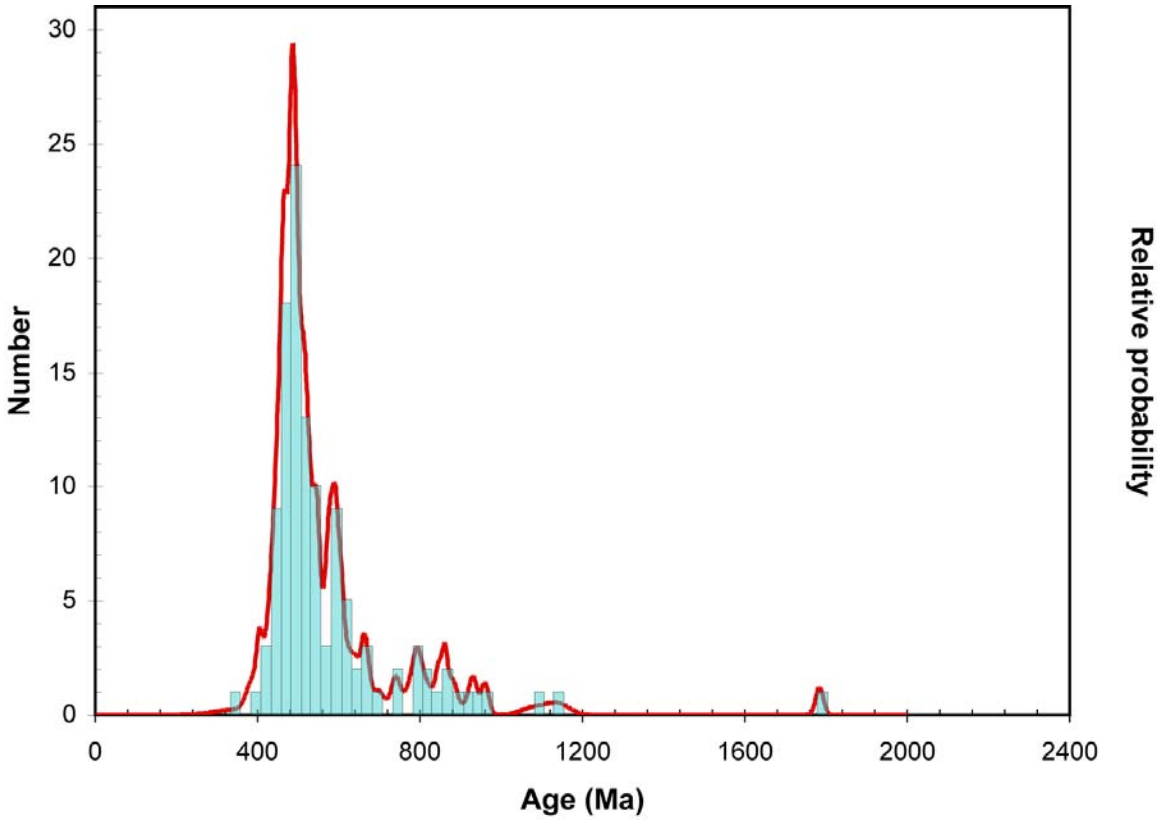

Figure 4.2. Detrital Muscovite $^{40}Ar/^{39}Ar$ Ages, Cumulative relative probability plot of all data from all samples. N = 119. Columns represent frequency of age within a 20 Ma age range, red line is a relative probability curve based on frequency.

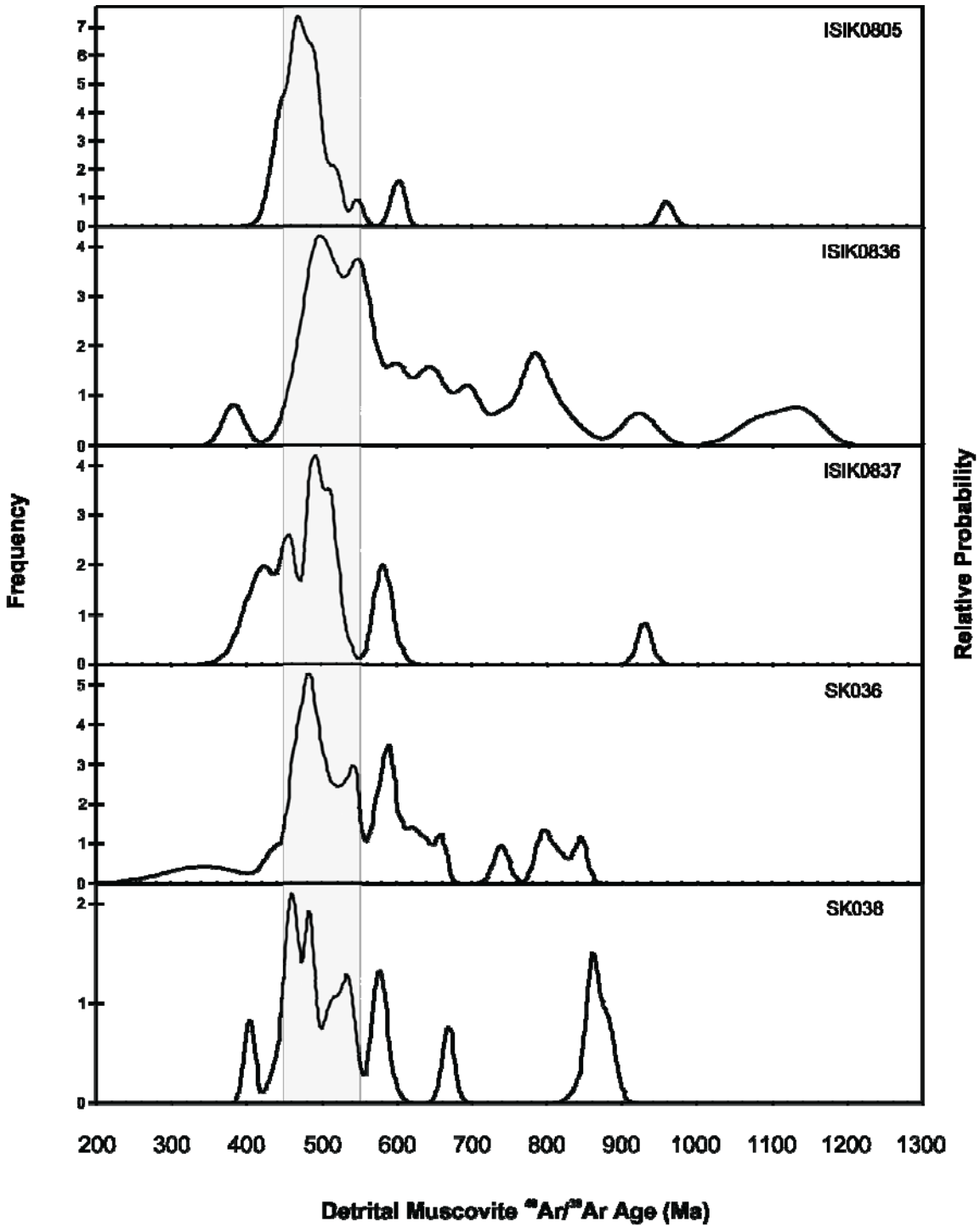

Figure 4.3. Detrital muscovite $^{40}Ar/^{39}Ar$ ages displayed in relative probability plots for the five samples from the Gondwana Formation of the LHS. The grey shaded area shows Cambrian-Ordovician time, where the majority of youngest peaks occur.

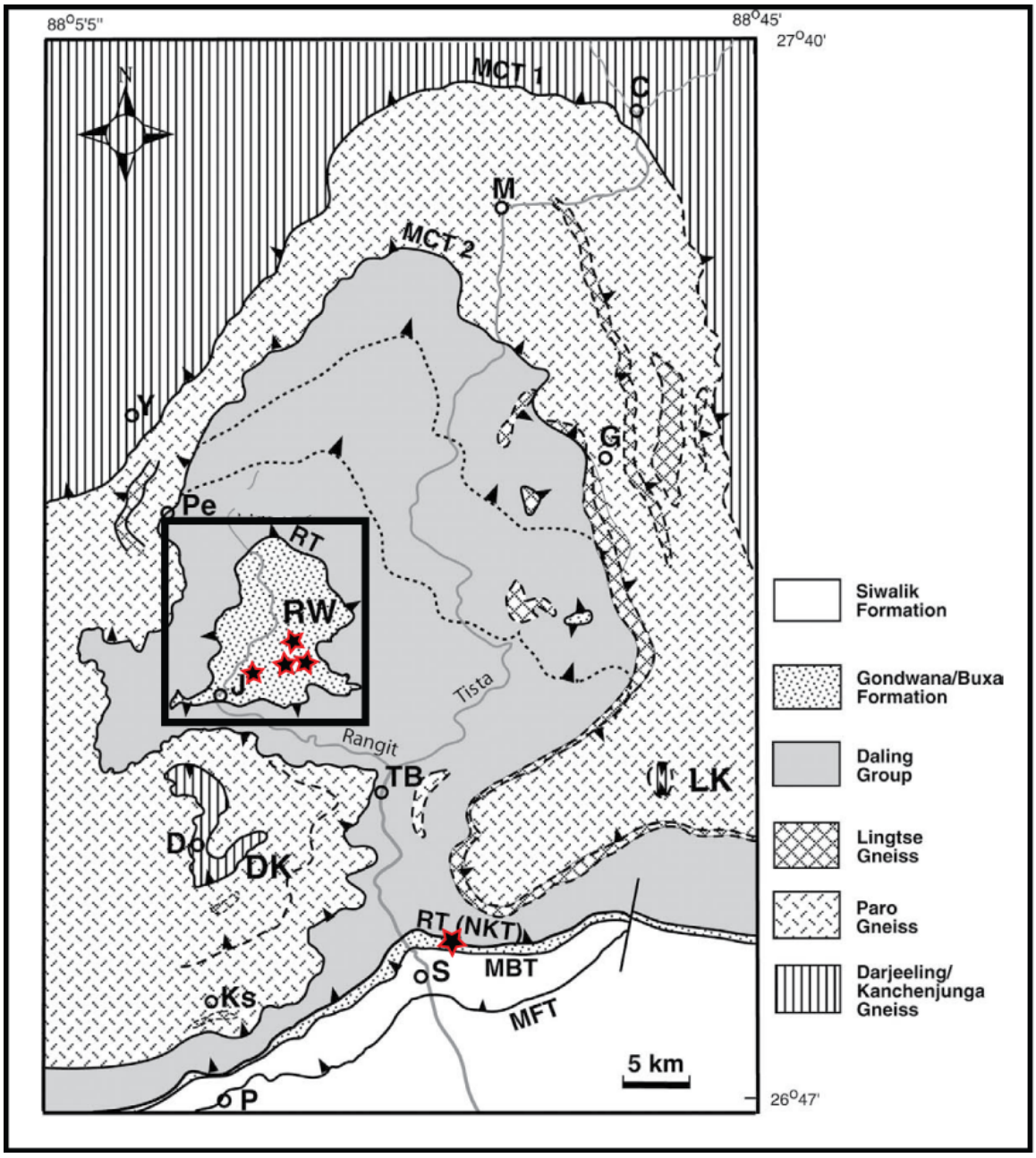

Figure 4.4. Regional map of the Darjeeling – Sikkim Himalaya (DSH), with georeferenced sample locations shown as stars, modified Bhattacharyya and Mitra, (2009). Towns shown are: C — Chungthang; D — Darjeeling; G — Gangtok; J — Jor khabari; Pe — Pelling ; S — Sevok; TB — Teesta Bazaar; and Y — Yuksom.

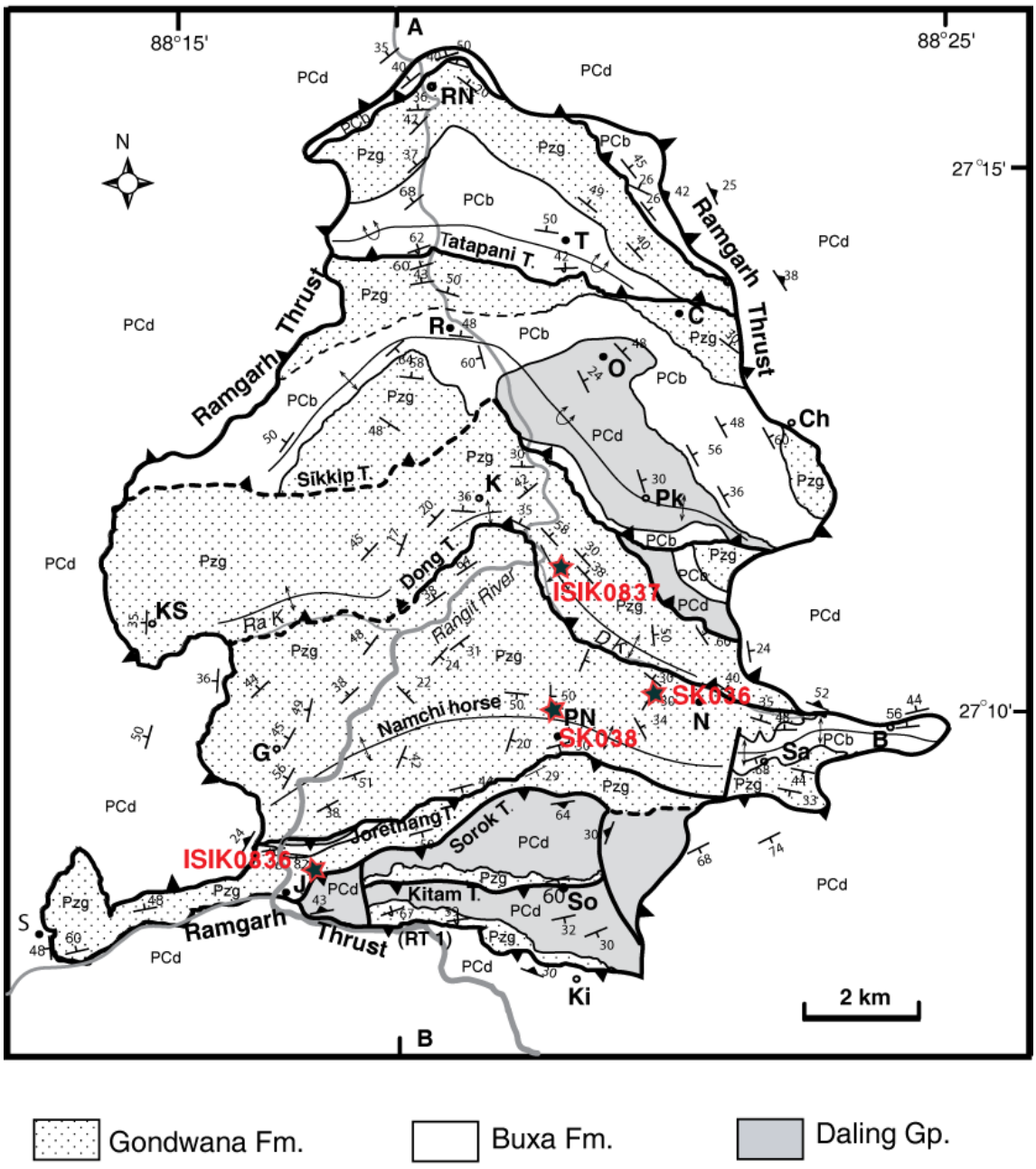

Figure 4.5. Map of the Rangit window showing the thrust slices constituting the Rangit duplex, as well as georeferenced sample locations shown as stars, modified after Bhattacharyya and Mitra, (2009). Towns are B—Banzyang, C—Chamchey, Ch—Chiyadaara, G—Gelling, J—Jorethang, K—Kamling, Ki—Kitam, KS—Khani Sabang, N—Namchi; O—Omchu, Pk—Pakzer, PN—Purana Namchi, R—Reshi, RN—Rangitnagar power station, S—Singrep, Sa—Samdong, So—Sorok, and T—Tinkitam. Small streams shown are RaK: Rathong Khola, DK: Dong Khola Sample ISIK05 is from the Gondwana formation along the orogenic front, the remaining four samples are within the Rangit window. ISIK0836 is located along the southen edge of the RW, SK36 and SK038 are located in the southeastern corner of the window and ISIK0837 is located in the eastern central area of the window.

One hundred-nineteen analyses were completed of individual muscovite grains separated from five samples from the Gondwana Formation (Figures 4.4 & 4.5). The individual ages range between 342.5 +/- 52.1 and 1783.6 +/- 9.5 Ma (Fig. 1). The compiled data display a unimodal distribution with a strong peak at 486 Ma, with the majority of the data occurring between 400 and 1000 Ma. There are four clusters centered at ca ~500, ~800-900, ~1100 and ~1800 Ma.

Twenty-seven analyses of muscovite from sample ISIK0805 provided ages between 432.9 +/- 9 and 959.8 +/- 9 Ma showing a fairly unimodal data distribution (Fig. 2). The data display a large peak at 470.25, which also corresponds to the youngest peak. The majority of the data are defined between 425-560 Ma, with a small peak at around 600 Ma and a third peak at~ 950 Ma.

For the sample ISIK0836, twenty-six analyses yielded ages between 382.9 +/- 14 and 1141.8 +/- 25.6 Ma, with the majority of the data between 450 and 800 Ma (Fig. 2). The data display a large and moderately wide two-tiered youngest peak, with the first tier occurring at 498.5 Ma and the second tier located at 548 Ma. There are also a series of smaller peaks between at ~ 800, ~950 and ~100 Ma with low frequencies.

Twenty-two analyses from sample ISIK0837 provided a large range of ages, between 400.5 +/- 20.4 and 1783.6 +/- 9.5 Ma. The majority of data are found between 400 and 600 Ma (Fig. 2). The data display a progressive gradual peak, followed by two small peaks. The youngest peak occurs at 457.5 Ma, followed by the most prominent peak located at 490.4 Ma. There are also smaller peaks located at 582.1 Ma and with a single outlier around 925 Ma, both displaying low frequencies. Note that the single grain analysis at 1783.6 +/- 9.5 Ma was not plotted for clarity of data presentation.

Twenty-eight analyses of muscovite from sample SK036 yielded ages between 342.5 +/- 52.1 and 845.6 +/- 8 Ma, with the majority of the data occurring between 450 and 650 Ma (Fig. 2). The data display a broad distribution with a moderately strong and youngest peak at 484.4 Ma and with a smaller multiple peak between 500-600 Ma.

Finally, sixteen analyses from sample SK038 produced ages between 404.1 +/- 6.8 and 881.2 +/- 10.2 Ma showing a broad distribution of data (Fig. 2). The majority of the data is between 450-600 Ma The youngest peak is two-tiered at 461.6 Ma and at 481.4 Ma, both of which are not strongly defined. A second cluster of ages occurring between 850-900 Ma defines a peak at 861.8 Ma.

CHAPTER 5 DISCUSSION

The muscovite $^{40}Ar/^{39}Ar$ ages are all pre-Tertiary and therefore provide (a) information about the provenance of the Gondwana sediments and thus shed light on the paleogeography of the Himalayan tectonostratigraphic units and (b) constraint on the maximum temperature and thus burial of the lowest unit in the core of one of the deepest tectonic windows of the Himalaya.

5.1. Provenance

The provenance of the detrital muscovite grains can be inferred from the Ordovician ages that were yielded from the grains, which suggests a magmatic or metamorphic source of similar age. However there are other 3 minor peaks. These minor peaks, ~800, ~900 and ~1100, correspond to peaks of detrital zircon U-Pb ages found within the Himalayas (McQuarrie et al., 2008). The lithological unit providing these muscovites cannot be demonstrated clearly.

5.1.1. Northern Sources

Muscovite is a common mineral associated with granite bodies and metamorphic rocks, and regularly occurs in sediments within a proximal area of its source. Based on this information and the ages determined from 40Ar/39Ar dating, an indication that the muscovite grains could have originated from a granitic host of a similar age within the catchment of rivers, bringing sediments to the Gondwana basins. There are occurrences

of granites with peraluminous compositions and U-Pb zircon ages ranging from 530 – 470 Ma (Cawood et al., 2007) found to the north of the study area. The nearest ones are within the Greater Himalayan Sequence and Tethyan Himalayan Sequence, ~300 km to the north/northeast of the Rangit window (Fig 5.1).

The ages of granitic bodies coincide with the ages of the youngest peak observed, and could be a possible origin for the detrital muscovite in the Gondwana Formation, provided that they were exposed within ~150 Ma of their emplacement. This would allow the detrital material to be transported and deposited by the Permian, the depositional age of the Gondwana Formation.

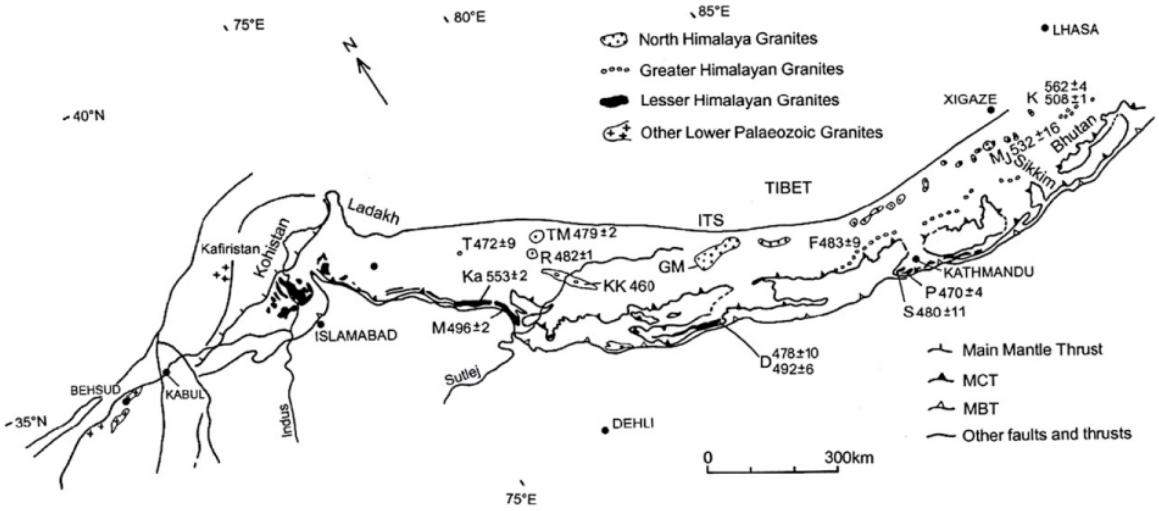

Figure 5.1. Map to show the distribution of Himalayan Cambro-Ordovician granites dated by the zircon and /or monazite U–Pb method. After Cawood et al., 2007.

Modern river sediments sampled from the Tista show further evidence that the source of the Gondwana sediments could have been sourced from the north. Cina et al. (2009) examined the age of detrital zircons that were collected from modern day river sand and from Neogene Siwaliks sediments within the eastern Himalaya. U-Pb ages of the detrital zircons from the Tista sediments revealed a prominent age peak at ~475 Ma, which

agrees with the ages calculated from this study. Although such rocks were not yet dated directly in the Sikkim Himalaya, this indicates there are outcrops of Cambrian-Ordovician granite in the catchment of the Tista, providing detrital material into the river systems that displays similar ages to the Gondwana samples. These units were however, supposed to have been located north of the reconstructed Gondwana basins (Fig. 5.2). If they are in the hanging wall of the MCT they were placed southward for at least a 100 km (McQuarrie et al., 2008), or according to modeling results on the order of 400 km (Jamieson et al., 2006) between points astride the MCT.

5.1.2. Shillong Plateau

The Cambrian-Ordovician granite bodies are not found solely to the north. According to Yin et al. (2010) similar aged bodies are found to the southeast of the study area on the Shillong Plateau of Eastern India. Yin et al conducted U-Pb zircon geochronology on granitic bodies found within the basement of the Shillong Plateau and obtained crystallization ages from 480-500 Ma These ages reflect very similar values as shown by Cina et al. (2009), Cawood et al. (2007) and this study, of Cambrian-Ordovician. The position of the Shillong Plateau is ~300 km southeast of the Rangit Window, and has not varied greatly through Himalayan orogeny because the estimated displacement along the MBT and duplexes of the Rangit window is on the order of ~ 142 km (Bhattacharyya and Mitre, 2009), which shows similar distance from a possible sediment source as the granitic bodies found to the north (Figure 5.1). The plateau could potentially have supplied the sediments that are found in the Gondwana succession, but originating from a more southern source.

Note that there are not only Cambrian-Ordovician granites on the Shillong Plateau, but also granites and gneisses of ages from 1.0 - 1.1 Ga (Yin et al., 2010), which compare to the oldest peaks obtained from my samples. Cina et al. (2007), have similar results which show Cambrian-Ordovician ages, as well as 800-900 Ma ages that coincide with smaller peaks obtained in the results. The ages obtained from Cawood et al. (2007) are similar ages that are found within the youngest peak of the majority of the samples, yet cannot account for the older ages that are observed in the smaller late age peaks.

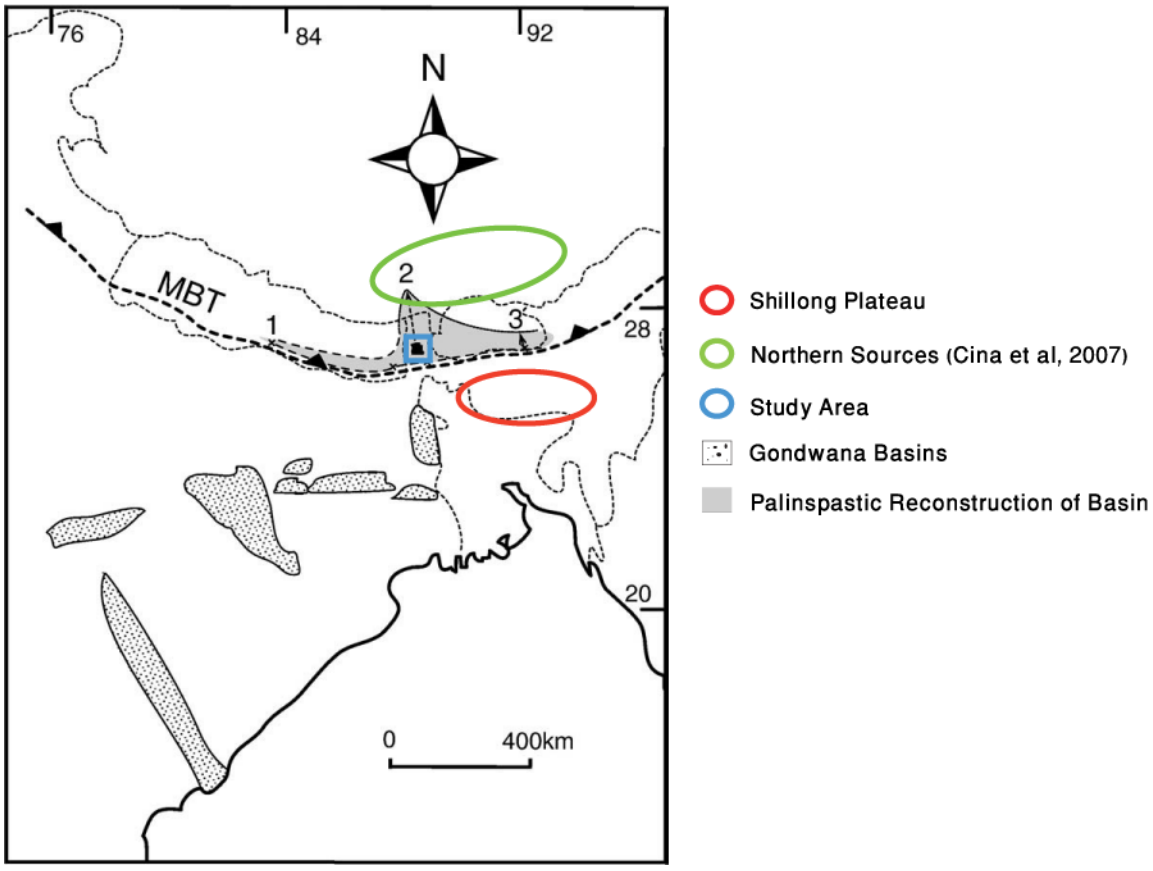

Figure 5.2. Map showing the major Gondwana basins of Peninsular India and the northern extent of the Gondwana basin in the eastern Himalaya. 1 Central Nepal, 2 the Rangit window and and Gondwana exposures in the foreland of the Darjeeling-Sikkim Himalaya and easternmost Nepal, 3 eastern Bhutan. The gray region shows the palinspastic reconstruction of the Gondwana basin from these exposures. Shillong Plateau outlined in red and northern sources outlined in green. After Bhattacharyya et al. (2009).

During the Permian era, Gondwana rift basins were created by failed rift systems in Peninsular India where sediment became deposited and where outcrops of the Gondwana succession can be found (Fig. 5.3) (Veevers and Tewar, 1995). Paleocurrent data from the Gondwana sediments in India indicate that the sediment that was supplied to these basins was transported from the south to the north (Veevers and Tewar, 1995). They also hypothesized that the sediment was transported from the radially draining paleo upland of the eastern Antarctic towards eastern India, eastern Africa and southwest Australia (Figure 5.3). This provides further evidence to the possibility of the Shillong Plateau acting as a source for the Gondwana Formation.

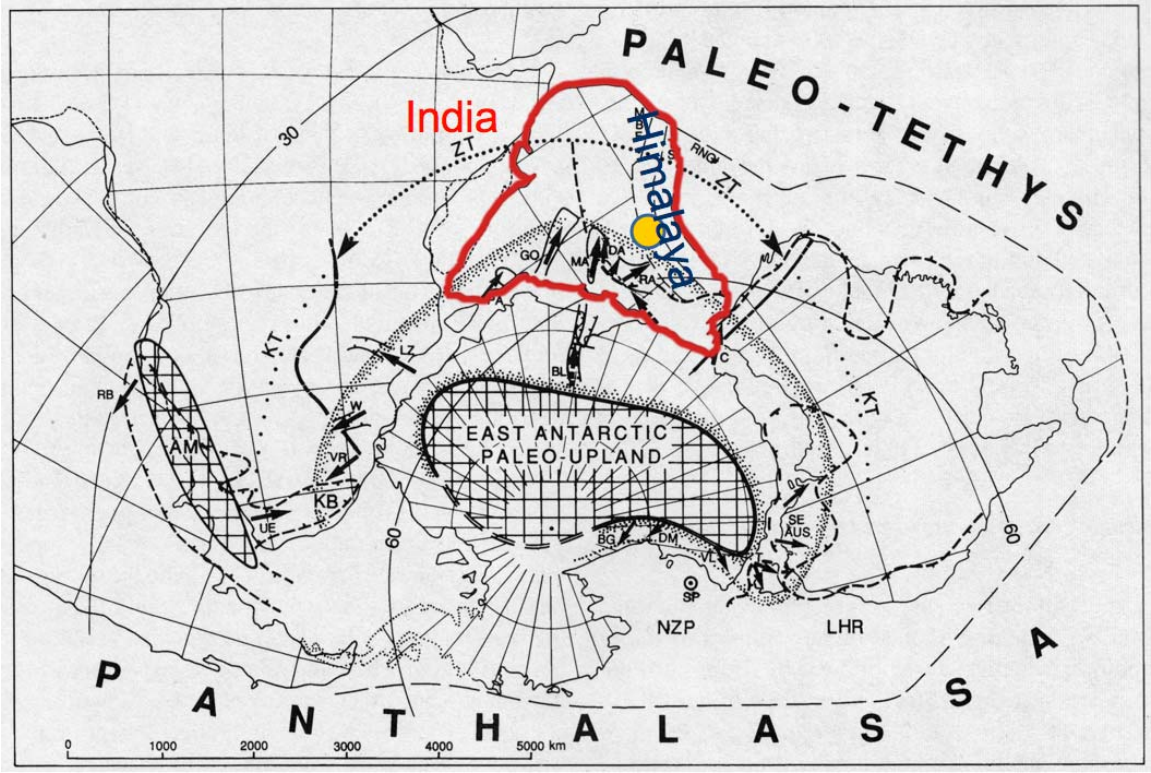

Figure 5.3. Reconstruction of Gondwanaland during the Permian, showing paleo current direction of the Gondwana basins with short black arrows. Yellow button indicates the Rangit window. After Veevers and Tewari (1995).

5.2. Constraints on Maximum Temperature in the Rangit Window.

In the Sikkim Himalaya the Ramgarh thrust, within the Lesser Himalayan Sequence, separates Gondwana and Buxa successions in the footwall from the Daling unit in the hanging wall. The thrust is well exposed in the Rangit Window and contains an asymmetrical repetition of the Daling-Buxa-Gondwana sequence from the Lesser Himalayan Sequence (LHS) called the Rangit duplex (Mitra et al., 2010). This is the result of a series of imbricate thrust wedges caused by the thrusting of the Ramgarh, which caused a total of 125 km of shortening in the LHS (Mitra et al., 2010). According to McQuarrie *et al.* (2008) a similar thrust in Bhutan displays the same type of duplexing found in the Rangit duplex, repeating sections of the LHS with the Ramgarh Thrust emplaced overtop. This thrust is called the Shumar thrust and is located between MBT and MCT, the same location as the Ramgarh in the Sikkim.

From the single grain muscovite $^{40}Ar/^{39}Ar$ age data, it is a clear that the muscovite grains from the Gondwana unit are not Permian in age, but are Ordovician based on the youngest peaks in the cumulative probability plots. This suggests that Tertiary metamorphic temperatures did not exceed the closure temperature of 425 °C and therefore the detrital muscovite did not experience any resetting of the $^{40}Ar/^{39}Ar$ system. If resetting were to occur, ages younger than the depositional age would be expected. There are clearly no suggestions of ages less than ~340 Ma for any sample (Fig. 4.2).

Plots from each sample in the results show ages younger than Cambrian-Ordovician, and could have two explanations. Because we do not see any ages indicated before the time of deposition for the Gondwana Formation, the younger grains could potentially show their true age. The complication is that we do not have evidence of a

source that could potentially have provided the young detrital muscovites. The other explanation is that a partial reset could have occurred in some of the samples, as they were close to the Ramgarh thrust. There are still smaller grains to be analyzed, which could help identify is this occurred, as smaller grains would be more susceptible to resetting, as they have a much lower closure temperature. However, we still do not see evidence for a full reset.

Further evidence that the muscovite rich Gondwana sediments did not exceed 425 °C, was provided by Whynot, (2010) using Raman spectroscopy on the carbonaceous material. From Daling sediments, a sample located within the footwall of the Shumar thrust of Bhutan (Figure 5.4), graphite grains yielded a maximum temperature of ~454.4 ± 10 °C. This indicates that the rocks in the hanging wall of the Shumar thrust reached a maximum temperature of ~465 °C. Within the hanging wall of the same thrust a temperature was calculated at 401.3 ± 6 °C. If the assumption is made that the Shumar thrust in Bhutan is the equivalent to the Ramgarh thrust in Sikkim, then the temperature achieved by the Ramgarh thrust in the hanging wall did not reach 425 °C and would not be high enough to reset the detrital muscovite grains analysed. The samples analysed for this thesis came from the hanging wall of the Ramgarh thrust which did not produce enough heat through metamorphic and tectonic processes to allow the muscovite grains to pass through their closure temperature, causing resetting.

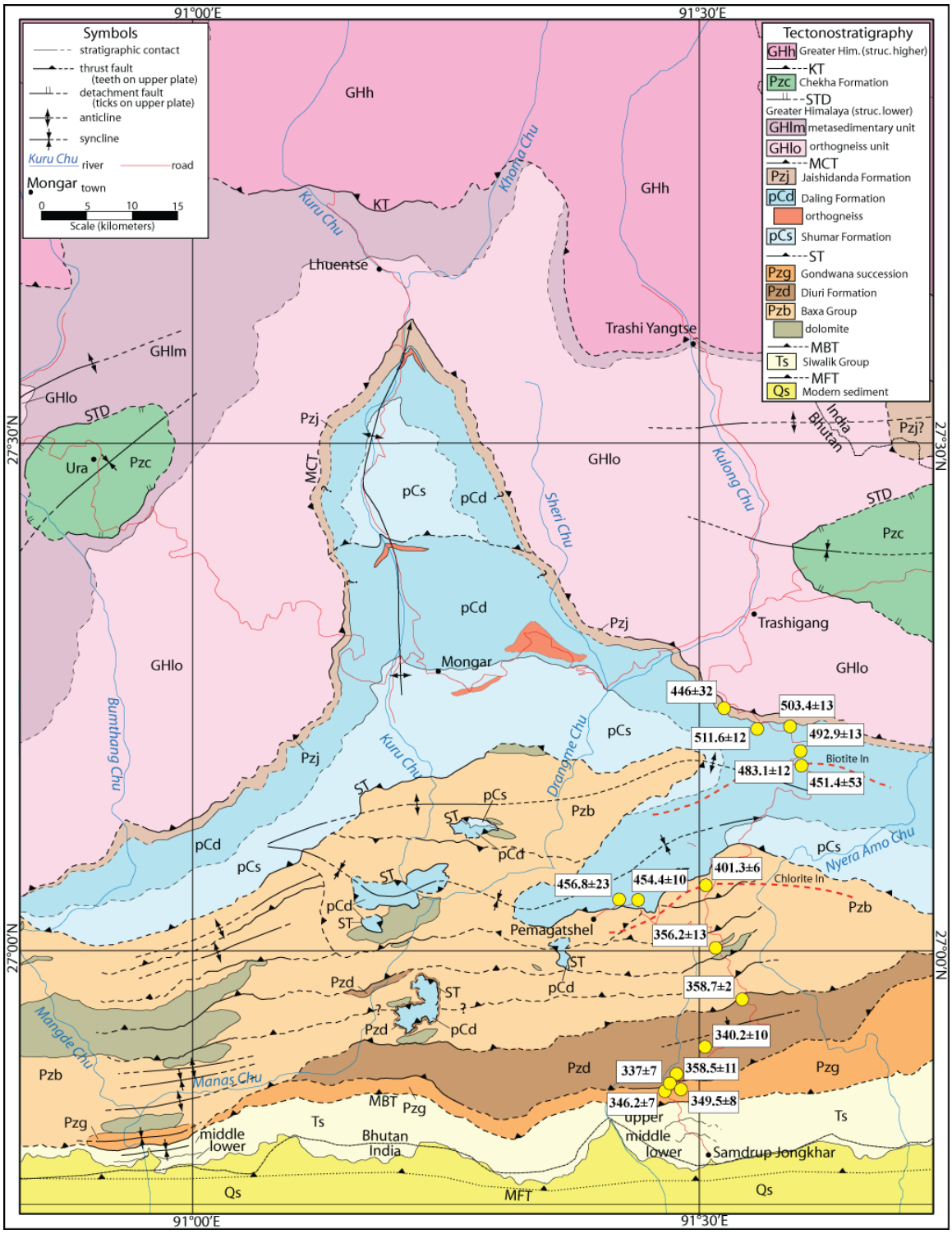

Figure 5.4. Geological map of the Kuru Chu Valley, Bhutan, with metamorphic temperatures calculated using Raman Spectroscopy from locations indicated in yellow. After Whynot, (2010), modified from McQuarrie et al. (2008)

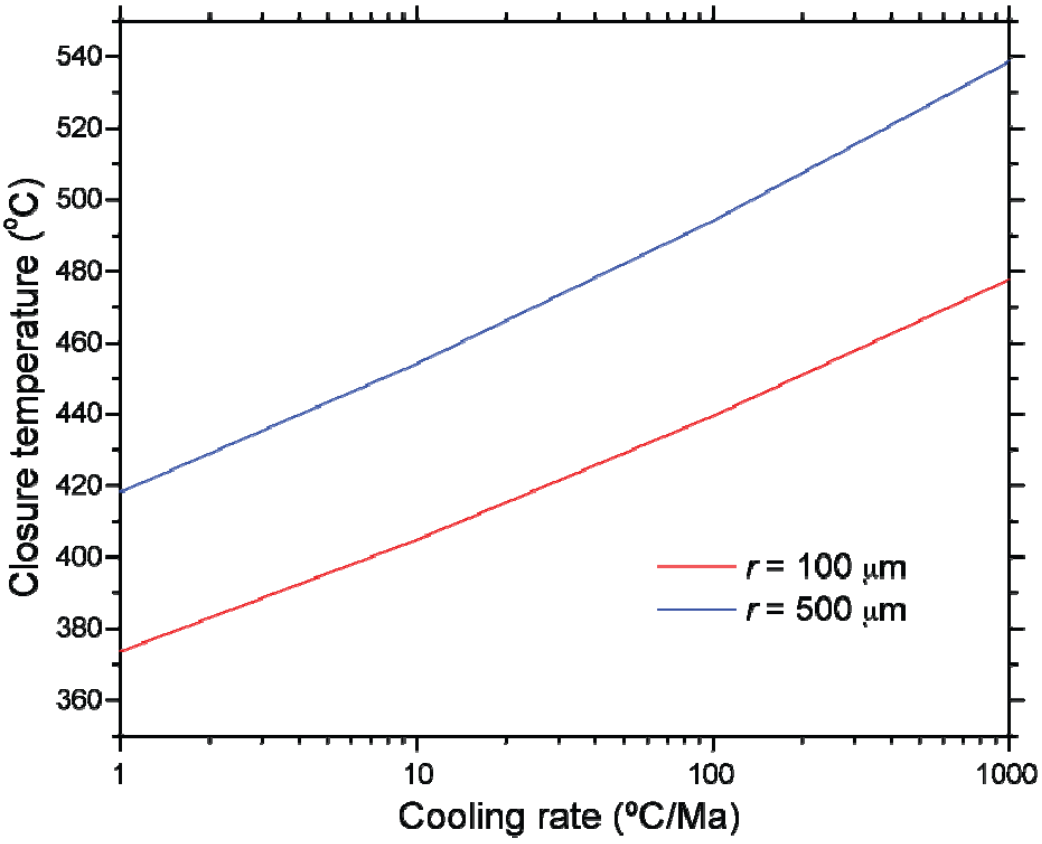

Figure 5.5. Variation of Tc of muscovite with cooling rate and diffusion dimension for Arrhenius parameters appropriate to 5kbar pressure (E = 64 kcal/mol and Do = 20 cm2/s). After Harrison et al., 2009.

The closure temperature of muscovite for the grain sized fractions that have been analyzed so far was thought to be ~425 °C, based on grain size alone (Harrison et al., 2009) (Fig. 5.5). However, for this closure temperature to be correct, the cooling rate of the muscovite grain would be very low, ~1.5 °C/Ma. We know that the grains are between ~500 μm and 1.0 mm, and this factor alone allows a minimum closure temperature of ~420 °C, associated with a cooling rate of ~1 °C/Ma. According to Kellet et al. (2009), in western Bhutan the area was calculated to pass through ~425 °C at ~11 Ma, based on $^{40}Ar/^{39}Ar$ muscovite ages. This provides a cooling rate of 38 °C/Ma, and if this value is used with the minimum grain size of 500 μm, then a closure temperature of

~475 °C can be inferred. We can assume that the cooling rate from $^{40}Ar/^{39}Ar$ muscovite ages has been maintained.

Using apatite fission track ages in western most Bhutan, (AUTHORS) calculated the area passed through the closure temperature of apatite, ~110 °C, between 2 and 4 Ma. Using this data, one can obtain cooling rates of 55 °C/Ma and 27.5 °C/Ma. These cooling rates then refer to muscovite closure temperatures with values ranging from 485 °C to 470 °C, respectively. A change was observed in eastern Bhutan, where ages of 4 – 8 Ma were determined passing through 110 °C. This results in cooling rates of 27.5 °C/Ma and 13.75 °C/Ma, and closure temperatures of 470 °C and 460 °C, respectively. As you approach central Nepal, the fission track ages of apatite reveal a cooling time of 0 – 2 Ma. This can then be attributed to cooling rates of 110 °C/Ma to 55 °C, assuming that these were continuous cooling rates, closure temperatures of ~500 °C and ~485 °C can be calculated. The east-west change across Bhutan that was observed has been attributed to elevation change, and the timing of erosion.

The maximum burial of the Gondwana Formation can also be estimated from the closure temperatures calculated. Based on grain size and cooling rate, the average range of closure temperatures for muscovite from this study has been estimated at 470 – 475 °C. If we assume extreme values in terms of geothermal gradients, then a range of depths can be calculated. The lower limit will be estimated at ~30 °C/km and the upper limit will be placed at 60 °C/km. Using these values, the maximum burial of the lowermost unit of the Gondwana Formation is estimated to be between 7.8 and 15.8 km (Figure 5.6).

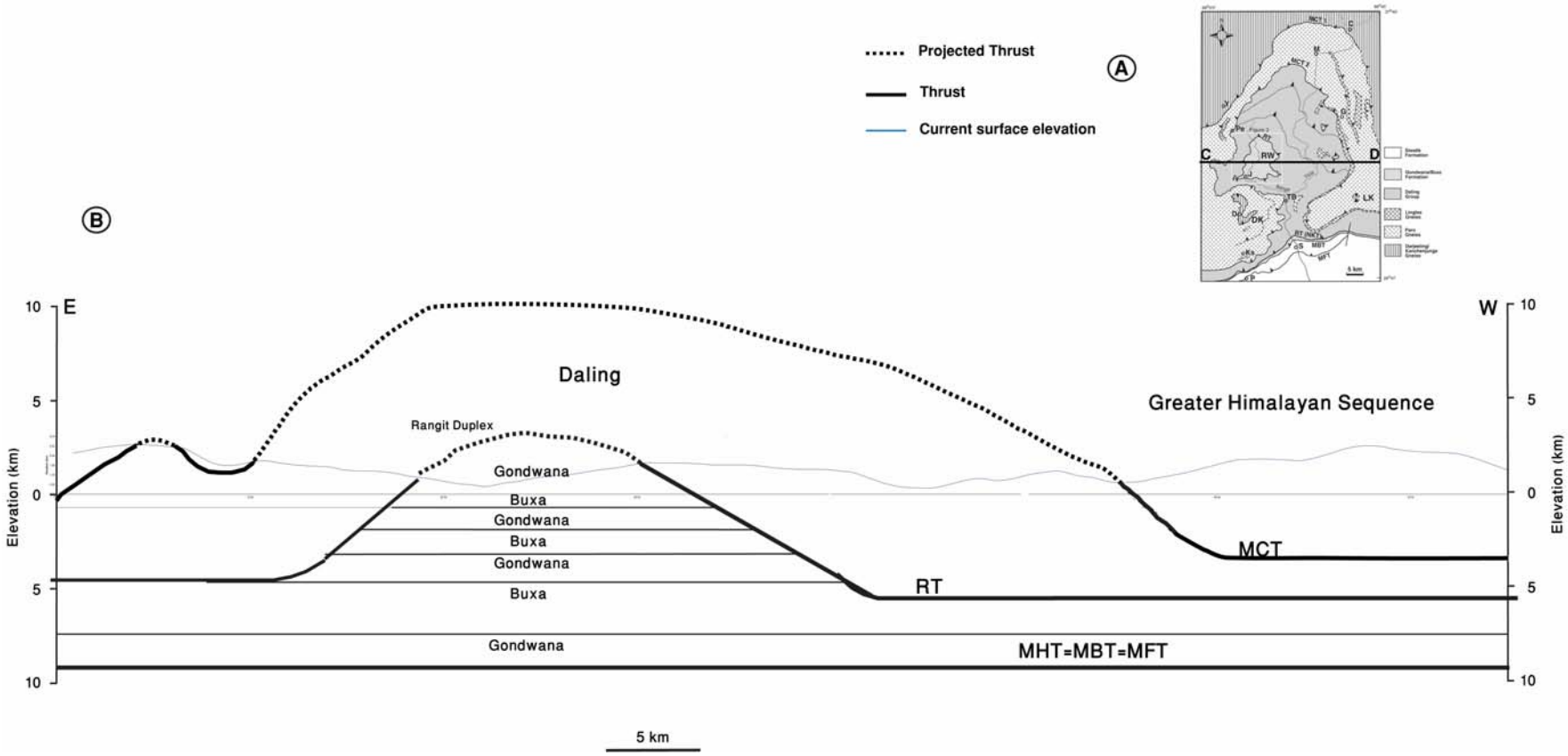

Figure 5.6. A) A regional map of the Darjeeling-Sikkim Himalaya, showing the location of the cross section C-D. Modified after Bhattacharyya and Mitra (2009). B) Cross section along C-D of Figure 5.6A showing the extent of maximum burial (~8 km) of the Gondwana Formation of the Lesser Himalayan Sequence. MCT – Main Central Thrust, RT – Ramgarh Thrust, MHT=MBT=MFT – The amalgamation of the Main Himalayan Thrust, Main Bounday Thrust and Main Frontal Thrust.

CHAPTER 6 CONCLUSION

From the work performed in this thesis, we can conclude that the maximum temperature that the detrital muscovite grains experienced was not high enough to exceed their closure temperature. However, the temperature that was achieved by the detrital muscovite grains is unknown. The age data obtained from the $^{40}Ar/^{39}Ar$ single grain total fusion clearly show all ages older than the Permian depositional age of the Gondwana Formation, with no indication of post-Tertiary aged grains. This also allows us to infer that the Tertiary burial temperatures within the Rangit window appear to have peaked at ~350 °C in the foot wall of the Ramgarh thrust and increased to < 450 °C in the hanging wall, by assuming that the Raman spectroscopy temperature data obtained by Whynot (2010) in eastern Bhutan and in the hanging wall of the Ramgarh thrust is consistent.

As there is no evidence for a resetting event, the source of the Cambrain-Ordovician muscovite grains could potentially have originated from granite bodies of similar ages observed along the entire Himalayan orogen (Cawood et al., 2007). There are also similar ages found in the basement of the Indian plate in the Himalayan foreland (Yin et al., 2010). Based on paleoflow evidence and reconstruction, by Veevers and Tewari (1995), the provenance of the sediment in the Gondwana Formation is thought to have originated from a northward-flowing Permian drainage system, supplying sediment to the various basins, from the basement rocks, that were infilling at the time.

The hypothesis of a partial reset is still something that needs to be considered, as only the largest grain size fractions of the detrital muscovite grains have been analyzed thus far. By dating the remaining smaller size fractions and utilizing intragrain traverse

analysis, an in depth look at the possibility of a partial resetting of the muscovite grains needs to be complete. With this additional information, it would provide a better understanding of the thermal effects of the Tertiary period, as well as provide further information about the provenance of the sediment and provide a better understanding about accurate closure temperatures for muscovite.

References

Bhattacharyya, K., and Mitra, G., 2009. A new kinematic evolutionary model for the growth of a duplex - an example from the Rangit duplex, Sikkim Himalaya, India. Gondwana Research 16 (3-4): 697-715.

Catlos, E.J., Dubey, C.S., Harrison, T.M., and Edwards, M.A., 2004. Late Miocene movement within the Himalayan Main Central Thrust shear zone, Sikkim, north-east India. Journal of Metamorphic Geology, 22, 207–226.

DeCelles, P.G., Robinson, D.M., Quade, J., Ojha, T.P., Garzione, C.N., Copeland, P., and Upreti, B. N., 2001. Stratigraphy, structure and tectonic evolution of the Himalayan fold– thrust belt in western Nepal. Tectonics 20, 487–509.

Dickin, Alan P. 2005. Radiogenic isotope geology. Cambridge: Cambridge University Press.

Faure, G. 1986. Principles of isotope geology. New York: Wiley.

Faure, G., Mensing, T.M. 2005. Isotopes: Principles and Applications. Hoboken, N.J. : Wiley.

Harrison, T.M., Celérier, J., Aikman, A.B., Hermann, J., and Heizler, M. Geochimica et Cosmochimica Acta 73 (4): 1039-1051.

Hodges, K. V. 2000. Tectonics Structure - OVERVIEW - Tectonics of the Himalaya and southern Tibet from two perspectives. Geological Society of America Bulletin 112 (3): 324.

Hollister, L. S., and Gruijic, D. 2006. Pulsed channel flow in Bhutan. Geological Society special publication 268: 415-424.

Joshi, A., 1989, Marine Permian fossils from the foothills of the Bhutan Himalaya: Current Science, v. 59, no. 6, p. 318-321.

Joshi, A., 1995, Setikhola Formation, in Bhargava, O.N., ed., The Bhutan Himalaya: A Geological Account: Geological Society of India Special Publication 39, p. 34-37.

Kellett, D.A., Grujic, D., and Erdmann, S. 2009. **Miocene structural reorganization of the south Tibetan detachment**, eastern Himalaya: Implications for continental collision. Lithosphere October 2009, v. 1, p. 259-281

Kuiper, K.F., Deino, A., Hilgen, F.J.,Krijgsman, W.,Renne, P.R. and Wijbrans, J.R. 2008. Synchronizing rock clocks of Earth history. Science, v. 320, p. 500-504.

Lakshminarayana, G., 1995, Damuda Subgroup, in Bhargava, O.N., ed., The Bhutan Himalaya: A Geological Account, Geological Society of India Special Publication 39, p. 29-33.

Liu, G., and Einsele, G. 1994. Sedimentary history of the Tethyan basin in the Tibetan Himalayas. Geologische Rundschau 83 (1): 32-61.

McDougall, I., and Harrison, T.M. 1999. Geochronology and thermochronology by the $^{40}Ar/^{39}Ar$ method. Oxford Monographs on Geology and Geophysics, no. 9. New York: Oxford University Press

McQuarrie, N., Robinson, D., Long, S., Tobgay, T., Grujic, D., Gehrels, G., and Ducea, M., 2008. Preliminary stratigraphy and structural architecture of Bhutan: implications for the along strike architecture of the Himalayan system. Earth and Planetary Science Letters 272, 105–117.

Mitra, G., Bhattacharyya, K., and Mukul, M. 2010. The Lesser Himalayan Duplex in Sikkim: Implications for Variations in Himalayan Shortening. Journal of the Geological Society of India 75 (1): 289-301.

Montgomery, D.R., and Stolar, D.B., 2006. Reconsidering Himalayan anticlines. Geomorphology 86, 4–15.

Mukul, M. 2000. The geometry and kinematics of the Main Boundary Thrust and related neotectonics in the Darjiling Himalayan fold-and-thrust belt, West Bengal, India. Journal of Structural Geology, 22 (9): 1261-1283.

Najman, Y. 2006. The detrital record of orogenesis: A review of approaches and techniques used in the Himalayan sedimentary basins. Earth-Science Reviews 74, 1–72.

Patro, P. K., and Harinarayana, T. 2009. Deep geoelectric structure of the Sikkim Himalayas (NE India) using magnetotelluric studies. Physics of the Earth and Planetary Interiors 173 (1-2): 171-176.

Pearson, O.N., and DeCelles, P.G., 2005. Structural geology and regional tectonic significance of the Ramgarh thrust, Himalayan fold–thrust belt of Nepal. Tectonics v. 24, no. 4,.TC4008.

Searle, M.P., and Scaillet, B. 2006. Mechanisms and timescales of felsic magma segregation, ascent and emplacement in the Himalaya. Geological Society Special Publication, 268 : 293-308.

Simpson, G. 2004. Role of river incision in enhancing deformation. Geology, 32 : 341-344.

Zhu, Bin. 2005. Age of Initiation of the India-Asia Collision in the East-Central Himalaya. The Journal of Geology, 113 (3): 265.

APPENDIX A

Table 4.1 – Summary of single grain total fusion.

IR LASER SINGLE-GRAIN MUSCOVITE ARGON SUMMARY

SPOT NO.	CODE NO.	^{39}Ar(mV)	AGE (Ma)±1σ	% ATM	^{37}Ar/^{39}Ar	^{36}Ar/^{40}Ar	^{39}Ar/^{40}Ar	% IIC	Age(mA)	Err(mA)	40*/39K	Err(abs.)
Sample SK036 with J = 0.002324 ± 2.323985E-05												
1	I70-1-1	7.8	845.6 ± 8	12.8	0	0.000434	0.003380	0	845.6742	8.0794	257.3762	3.080213
2	I70-2-1	8.8	591.1 ± 5.6	4.2	0	0.000144	0.005721	0	591.1659	5.6617	166.8810	1.874423
3	I70-4-1	3.6	479.7 ± 9.9	4.8	0	0.000163	0.007200	0	479.7411	9.9851	131.1076	3.107771
4	I70-5-1	6	462.4 ± 7	3.2	0	0.000108	0.007657	0	462.4489	7.0676	125.7512	2.178733
5	I70-6-1	1.1	342.5 ± 52.1	79.5	0	0.002672	0.002256	0	342.5129	52.1403	89.9809	15.039330
6	I70-7-1	4.5	739.3 ± 10	12.3	0	0.000415	0.004008	0	739.3900	10.0660	218.0267	3.618019
7	I70-8-1	2.3	520 ± 12.5	1.2	0	0.000040	0.006792	0	520.0462	12.5928	143.7933	4.007961
8	I70-10-1	4.9	621.7 ± 8.1	1.8	0	0.000062	0.005517	0	621.7986	8.1102	177.1093	2.731075
9	I70-11-1	4.8	484.5 ± 8.3	1.9	0	0.000066	0.007349	0	484.5431	8.3917	132.6041	2.618797
10	I70-12-1	8.9	545.1 ± 5.9	1.2	0	0.000040	0.006487	0	545.1953	5.9403	151.8536	1.917190
11	I70-13-1	2.5	502.2 ± 11.7	3.9	0	0.000132	0.006882	0	502.2453	11.7480	138.1557	3.702361
12	I70-14-1	1.3	439.2 ± 14.3	4.2	0	0.000139	0.007899	0	439.2843	14.3301	118.6559	4.361171
13	I70-15-1	4.3	469.5 ± 9	3	0	0.000101	0.007529	0	469.5241	9.0967	127.9366	2.815265
14	I70-16-1	5.1	604.5 ± 8.8	2.4	0	0.000084	0.005667	0	604.5843	8.8478	171.3400	2.951124
15	I70-17-1	6.1	659.6 ± 7.2	2.9	0	0.000100	0.005090	0	659.6813	7.2808	190.0010	2.503793
16	I70-18-1	3.4	581.3 ± 10.9	3.1	0	0.000106	0.005880	0	581.3196	10.9137	163.6300	3.593562
17	I70-19-1	4.8	498.3 ± 7.8	1.8	0	0.000060	0.007131	0	498.3286	7.8950	136.9226	2.482679
18	I70-20-1	6.9	487.8 ± 6.5	2.7	0	0.000092	0.007248	0	487.8724	6.5649	133.6441	2.052480
19	I70-21-1	2	814.2 ± 15.4	4	0	0.000137	0.003877	0	814.2802	15.4111	245.5110	5.774005
20	I70-22-1	4.2	793.4 ± 9.5	2.2	0	0.000075	0.004096	0	793.4136	9.5531	237.7380	3.538064
21	I70-23-1	4.4	639.4 ± 9.1	2.9	0	0.000098	0.005278	0	639.4163	9.1802	183.0710	3.121719
22	I70-24-1	2.9	581.2 ± 11.8	6.4	0	0.000217	0.005674	0	581.2938	11.8028	163.6215	3.886274
23	I70-25-1	1.8	471.6 ± 14.1	9.8	0	0.000328	0.006914	0	471.6024	14.1788	128.5802	4.393144
24	I70-26-1	1.3	538 ± 16.3	9.2	0	0.000308	0.005965	0	538.0490	16.3532	149.5518	5.256994
25	I70-27-1	1.7	510.3 ± 14.8	2	0	0.000069	0.006853	0	510.3548	14.8963	140.7172	4.715684
26	I70-28-1	5.4	478 ± 7.7	2.8	0	0.000096	0.007399	0	478.0282	7.7100	130.5747	2.397397

27	I70-29-1	4.1	536.3 ± 9	2.6	0	0.000090	0.006492	0	536.3102	9.0991	148.9931	2.922227
28	I70-30-1	1.7	580.1 ± 15.4	6	0	0.000203	0.005681	0	580.1261	15.4821	163.2372	5.094424
	Sample SK038 with *J* = 0.002335 ± 2.334952E-05											
1	I72-1-1	6.5	668.7 ± 8.1	8.2	0	0.000274	0.005606	0	668.78	8.0759	192.2283	2.778128
2	I72-2-1	2.4	860.2 ± 15.2	13.9	0	0.000470	0.003270	0	860.27	15.2697	261.7228	5.841123
3	I72-3-1	4.9	535.9 ± 8.5	2	0	0.000067	0.006578	0	535.98	8.5394	148.1857	2.729065
4	I72-4-1	3.7	511.3 ± 9.9	6.6	0	0.000224	0.006603	0	511.39	9.9692	140.3816	3.142862
5	I72-5-1	7.6	463.5 ± 6.1	2	0	0.000070	0.007770	0	463.60	6.1373	125.5113	1.884235
6	I72-6-1	1.5	528.6 ± 15.2	1.7	0	0.000056	0.006626	0	528.63	15.2511	145.8412	4.854205
7	I72-7-1	4	881.2 ± 10.2	2.6	0	0.000087	0.003597	0	881.21	10.2799	269.7794	3.978294
8	I72-8-1	2.7	580.7 ± 11.9	2.9	0	0.000097	0.005920	0	580.71	11.9235	162.6606	3.906237
9	I72-9-1	4.9	575.5 ± 8.3	2.9	0	0.000099	0.006000	0	575.50	8.3784	160.9562	2.736929
10	I72-10-1	7.4	456.4 ± 6.3	4.2	0	0.000142	0.007734	0	456.44	6.3926	123.3176	1.954828
11	I72-11-1	4.8	487.5 ± 8.7	4.8	0	0.000164	0.007114	0	487.58	8.7243	132.9242	2.714327
12	I72-12-1	5.2	472.5 ± 8.3	6.7	0	0.000228	0.007228	0	472.59	8.3062	128.2788	2.562852
13	I72-13-1	6.2	404.1 ± 6.8	3.9	0	0.000131	0.008885	0	404.17	6.8335	107.5639	2.029987
14	I72-14-1	9.3	484.4 ± 5.3	2.2	0	0.000077	0.007382	0	484.43	5.3277	131.9448	1.654685
15	I72-15-1	8.6	860.9 ± 6.3	1.3	0	0.000045	0.003758	0	860.94	6.3110	261.9800	2.415025
16	I72-16-1	2.5	447.8 ± 12.7	8.7	0	0.000294	0.007472	0	447.84	12.7809	120.6951	3.889789
	Sample ISIK0805 with *J* = 0.002348 ± 2.347946E-05											
1	I74-1-1	4.1	432.9 ± 9	7.2	0	0.000243	0.007969	0	432.96	9.076994	115.5406	2.724656
2	I74-2-1	6	474.7 ± 7.6	6.9	0	0.000233	0.007225	0	474.75	7.663289	128.2312	2.354218
3	I74-3-1	5.4	547.9 ± 7.9	3.1	0	0.000106	0.006375	0	548.00	7.987162	151.1970	2.555409
4	I74-4-1	5	488.4 ± 8.4	5.3	0	0.000180	0.007105	0	488.49	8.431441	132.4690	2.610009
5	I74-5-1	5.5	508.2 ± 8	3.6	0	0.000124	0.006913	0	508.29	8.089309	138.6307	2.531733
6	I74-6-1	7.7	524.7 ± 6.2	1.7	0	0.000059	0.006809	0	524.71	6.214330	143.7932	1.962702
7	I74-7-1	6.4	446.3 ± 7.2	3.4	0	0.000117	0.008032	0	446.37	7.281362	119.5825	2.201974
8	I74-8-1	4.6	486.7 ± 8.8	6	0	0.000202	0.007081	0	486.78	8.838678	131.9402	2.733481
9	I74-9-1	3.9	472 ± 9.7	7.3	0	0.000245	0.007225	0	472.03	9.742012	127.3977	2.988315
10	I74-10-1	6.2	494 ± 6.9	4.5	0	0.000153	0.007081	0	494.08	6.997559	134.2028	2.172867
11	I74-11-1	7.1	606.3 ± 6.6	2.6	0	0.000090	0.005701	0	606.39	6.639703	170.1835	2.194193
12	I74-12-1	6.5	464.9 ± 6.8	4.2	0	0.000144	0.007609	0	464.96	6.854050	125.2314	2.094215
13	I74-13-1	5.5	493.5 ± 7.7	3.9	0	0.000131	0.007134	0	493.51	7.795624	134.0246	2.419911

14	I74-14-1	5.2	444.7 ± 7.8	4.5	0	0.000151	0.007972	0	444.74	7.893649	119.0878	2.384972
15	I74-15-1	4.6	959.8 ± 9	2.2	0	0.000075	0.003258	0	959.85	9.027648	299.2219	3.629156
16	I74-16-1	2.3	462.2 ± 12.8	9.3	0	0.000312	0.007205	0	462.22	12.863180	124.3953	3.924306
17	I74-17-1	5.8	597.5 ± 7.5	4.1	0	0.000138	0.005710	0	597.57	7.576915	167.2785	2.491707
18	I74-18-1	1	447.8 ± 17.3	11.6	0	0.000383	0.007175	0	447.81	17.322930	120.0164	5.242838
19	I74-19-1	1.8	449.9 ± 15	13.3	0	0.000445	0.007074	0	449.97	15.050650	120.6703	4.560581
20	I74-20-1	5	468.7 ± 8.5	7.3	0	0.000247	0.007288	0	468.77	8.512627	126.3993	2.606495
21	I74-21-1	4.9	462.3 ± 8.2	5.2	0	0.000175	0.007571	0	462.35	8.253043	124.4355	2.518027
22	I74-22-1	3	468 ± 11.6	7.3	0	0.000245	0.007279	0	468.04	11.684750	126.1754	3.576322
23	I74-23-1	4.1	478.1 ± 8.9	5.8	0	0.000196	0.007234	0	478.17	8.913966	129.2836	2.743636
24	I74-24-1	3.3	486.9 ± 10.3	6.1	0	0.000208	0.007049	0	486.94	10.306700	131.9890	3.187765
25	I74-25-1	3.8	494.8 ± 9.7	6.7	0	0.000226	0.006889	0	494.82	9.705916	134.4309	3.015088
26	I74-26-1	1.1	470.4 ± 18.7	15.9	0	0.000529	0.006480	0	470.44	18.728030	126.9109	5.739677
27	I74-27-1	6.4	516.4 ± 6.8	3.9	0	0.000132	0.006776	0	516.46	6.858688	141.1948	2.156332
	Sample ISIK0836 with J = 0.002358 ± 2.35796E-05											
1	I76-1-1	2.9	548.9 ± 13.2	20.1	0	0.000678	0.005261	0	548.97	13.2297	150.8666	4.217042
2	I76-2-1	0.9	1141.8 ± 25.6	19.2	0	0.000647	0.002139	0	1141.80	25.6504	374.5880	11.357630
3	I76-3-1	2.5	600.4 ± 12.9	17	0	0.000573	0.004921	0	600.46	12.9462	167.5159	4.246153
4	I76-4-1	1.5	645.5 ± 17.7	18.6	0	0.000625	0.004417	0	645.58	17.7661	182.5018	5.974622
5	I76-5-1	1.6	480.1 ± 18.6	28.3	0	0.000949	0.005480	0	480.20	18.6391	129.3575	5.719029
6	I76-6-1	1.6	382.9 ± 14	18.7	0	0.000625	0.007971	0	382.98	14.0401	100.3160	4.081873
7	I76-7-1	1.3	512.3 ± 14.9	4.2	0	0.000141	0.006767	0	512.31	14.9807	139.2982	4.679082
8	I76-8-1	0.7	493.9 ± 19.3	11.9	0	0.000395	0.006411	0	493.98	19.3557	133.6019	5.984448
9	I76-9-1	1	549.7 ± 18.9	11.7	0	0.000390	0.005735	0	549.79	18.9004	151.1285	6.027340
10	I76-10-1	0.6	818.3 ± 27.5	15.1	0	0.000504	0.003421	0	818.35	27.5744	243.4738	10.205180
11	I76-11-1	1.4	509.4 ± 15.8	15.1	0	0.000504	0.006051	0	509.48	15.8453	138.4167	4.941385
12	I76-12-1	0.9	745 ± 21.8	6.3	0	0.000212	0.004252	0	745.09	21.8280	216.9062	7.756955
13	I76-13-1	0.4	1086.5 ± 32.1	7.8	0	0.000260	0.002586	0	1086.51	32.1098	350.4754	13.788540
14	I76-14-1	1.9	780.9 ± 13.9	6.5	0	0.000220	0.004039	0	780.93	13.9822	229.7696	5.068537
15	I76-15-1	0.5	621.3 ± 24.9	1	0	0.000033	0.005486	0	621.39	24.9517	174.4184	8.279259
16	I76-16-1	0.8	922.2 ± 22.4	4.1	0	0.000139	0.003344	0	922.29	22.4492	283.0736	8.801197
17	I76-17-1	0.7	569.5 ± 20	7.1	0	0.000236	0.005755	0	569.52	20.0553	157.4529	6.465943
18	I76-18-1	0.9	549.8 ± 17.2	4.1	0	0.000135	0.006214	0	549.86	17.2696	151.1484	5.507481

19	I76-19-1	1.1	791.2 ± 19.3	2.9	0	0.000100	0.004105	0	791.21	19.3351	233.5076	7.049004
20	I76-20-1	2	491.5 ± 11.5	2.1	0	0.000071	0.007284	0	491.57	11.5920	132.8571	3.579277
21	I76-21-1	1.2	522 ± 16.1	7.6	0	0.000255	0.006376	0	522.06	16.1755	142.3525	5.079669
22	I76-22-1	0.6	552.6 ± 20.1	0.2	0	0.000009	0.006350	0	552.70	20.1832	152.0557	6.446801
23	I76-23-1	0.3	496.3 ± 24.8	6.4	0	0.000206	0.006544	0	496.39	24.8141	134.3469	7.682357
24	I76-24-1	0.7	471 ± 20.3	17.1	0	0.000563	0.006380	0	471.06	20.3470	126.5616	6.211540
25	I76-25-1	0.3	664.6 ± 29.4	9.6	0	0.000310	0.004571	0	664.61	29.4783	188.9356	10.018510
26	I76-26-1	1.7	696.4 ± 14.5	1.9	0	0.000064	0.004862	0	696.49	14.5738	199.8667	5.041390
	Sample ISIK0837 with *J* = .00231 ± 2.310038E-05											
1	I68-1-1	4.6	1783.6 ± 9.5	2.1	0	0.000071	0.001337	0	1783.6160	9.5493	730.7821	6.160718
2	I68-2-1	5.3	494.9 ± 7.6	2.4	0	0.000083	0.007100	0	494.9209	7.6608	136.6754	2.419080
3	I68-3-1	3.7	452.9 ± 9.2	4.4	0	0.000148	0.007672	0	452.9544	9.2875	123.5765	2.865295
4	I68-5-1	9	482.9 ± 5.4	1	0	0.000036	0.007417	0	482.9975	5.4589	132.9228	1.712430
5	I68-6-1	2.7	496.5 ± 11.6	6.6	0	0.000222	0.006742	0	496.5529	11.6852	137.1910	3.693197
6	I68-7-1	8	513.7 ± 6.2	2.5	0	0.000086	0.006808	0	513.7767	6.2325	142.6608	1.988738
7	I68-9-1	4.2	584 ± 9.1	3.5	0	0.000120	0.005795	0	584.0202	9.1371	165.5171	3.031349
8	I68-10-1	3	505.3 ± 10.8	5.8	0	0.000196	0.006670	0	505.3727	10.8206	139.9854	3.436691
9	I68-11-1	2.2	408.1 ± 13.8	16.4	0	0.000548	0.007505	0	408.1202	13.8534	109.9152	4.168993
10	I68-12-1	7	490.8 ± 6.6	4.8	0	0.000165	0.006997	0	490.8788	6.6691	135.4005	2.101218
11	I68-13-1	2.4	429.9 ± 12.5	13.5	0	0.000453	0.007331	0	429.9576	12.5944	116.5268	3.836290
12	I68-14-1	2.7	400.5 ± 20.4	54.3	0	0.001829	0.004214	0	400.5721	20.4750	107.6484	6.135962
13	I68-15-1	2.1	427.8 ± 13.3	12.8	0	0.000430	0.007420	0	427.8846	13.3616	115.8957	4.065298
14	I68-16-1	3.3	525.7 ± 10.4	5.3	0	0.000181	0.006412	0	525.7315	10.4965	146.4882	3.371615
15	I68-17-1	5.7	461.5 ± 7.2	5.7	0	0.000193	0.007430	0	461.5011	7.2543	126.2195	2.248665
16	I68-18-1	3.9	451.4 ± 9.4	9.8	0	0.000329	0.007274	0	451.4118	9.4911	123.1008	2.925611
17	I68-19-1	4.2	511.9 ± 9.1	5.8	0	0.000196	0.006588	0	511.9118	9.1346	142.0660	2.911772
18	I68-20-1	2.3	494.4 ± 13.3	10.9	0	0.000366	0.006455	0	494.4579	13.3214	136.5292	4.205450
19	I68-21-1	5.7	929.9 ± 9.6	2.9	0	0.000098	0.003316	0	929.9276	9.6302	292.0184	3.870324
20	I68-22-1	2.3	588.9 ± 13.1	7.5	0	0.000253	0.005483	0	588.9226	13.1799	167.1457	4.384495
21	I68-23-1	2.6	475.4 ± 11.7	7.5	0	0.000252	0.007012	0	475.4571	11.7423	130.5624	3.668106
22	I68-24-1	4.2	573.7 ± 9.8	8.6	0	0.000290	0.005609	0	573.7369	9.8873	162.1152	3.261599

Table 4.2 – GPS coordinates of the samples from Sikkim

Sample number	N	E	H [m]
SK-36	27° 09.845	88° 21.205	1452
SK-38	27° 09.675	88° 19.978	1097
ISIK08-05	26° 55.462	88° 27.292	180
ISIK08-36	27° 08.101	88° 16.770	326
ISIK08-37	27° 11.089	88° 19.026	457